Correspondence to:
J. Ahrens,
janis.ahrens@uol.de

Seasonality of Organic Matter Degradation Regulates Nutrient and Metal Net Fluxes in a High Energy Sandy Beach

Janis Ahrens[1], Melanie Beck[1], Hannah K. Marchant[2], Soeren Ahmerkamp[2,3], Bernhard Schnetger[1], and Hans-Jürgen Brumsack[1]

[1]Institute for Chemistry and Biology of the Marine Environment, Carl-von-Ossietzky University of Oldenburg, Oldenburg, Germany, [2]Max Planck Institute for Marine Microbiology, Bremen, Germany, [3]Marum Center for Marine Environmental Sciences, Bremen, Germany

Abstract During seawater circulation in permeable intertidal sands, organic matter degradation alters the composition of percolating fluids and remineralization products discharge into surficial waters. Concurrently, coastal seawater nutrient and organic matter composition change seasonally due to variations in pelagic productivity. To assess seasonal changes in organic matter degradation in the intertidal zone of a high energy beach (Spiekeroog Island, southern North Sea, Germany), we analyzed shallow pore waters for major redox constituents (oxygen [O_2], manganese [Mn], and iron [Fe]) and inorganic nitrogen species (nitrite [NO_2^-], nitrate [NO_3^-], and ammonium [NH_4^+]) in March, August, and October. Surface water samples from a local time series station were used to monitor seasonal changes in pelagic productivity. O_2 and NO_3^- were the dominating pore water constituents in March and October. Dissolved Mn, Fe, and NH_4^+ were more widely distributed in August. Seasonal changes in seawater temperature as well as organic matter and nitrate supply by seawater were assumed to affect microbial rates and degradation pathways. Pore water and seawater variability led to seasonally changing constituent effluxes to surface waters. Mn, Fe, and NH_4^+ effluxes are minimal in March and reached their maximum in August. Furthermore, the intertidal sands switched from a net dissolved inorganic nitrogen sink in March to a net source in August. In conclusion, seasonal effects on intertidal pore water biogeochemistry affect constituent fluxes across the sediment-water interface. The seasonality of the beach bioreactor must be considered when fluxes are extrapolated to annual timescales.

Plain Language Summary Beach sands are biologically active environments. Seawater is circulated through the sandy beach (e.g., via waves or tides) as are nutrients and algal remains — organic matter. Subsurface microbes start to break down organic matter and change the pore water chemistry before it is reintroduced into the ocean. This so called bioreactor is affected by seasonal changes in temperature and algal activity controlling seawater nutrient and organic matter content. This affects the rates of organic matter break down. Microbes are adapted to break down organic matter using various pathways and energy sources. The seasonality determines how fast microbes exhaust their energy source, for example, oxygen. The respective reaction pathways influence the release of pore water nutrients and trace metals.

For example, beach sands of Spiekeroog are a sink for nitrogen in winter and early spring and retain nitrate from North Sea waters. In contrast, the beach is a nitrogen source to ocean water in summer: Nitrogen from algal biomass is recycled by microbes and resupplied to the coastal ocean. This is crucial, because during summer, nitrogen is a limiting factor for algal growth. Especially when coastal nutrient and metal budgets are being calculated, seasonal dynamics need to be considered.

1. Introduction

Worldwide, about one third of ice-free shorelines are covered by sandy beaches (Luijendijk et al., 2018) and many are exposed to mesotidal to macrotidal conditions (Flemming, 2005). The subterranean estuaries of these high energy beaches are complex and dynamic environments due to pore water advection. Wave pumping and bottom water currents cause advective pore water flow within surficial sediments, while tidal pumping induces advective flow into deeper layers (Santos et al., 2012). Combined with fresh groundwater discharge, these factors often shape a seawater circulation cell (Robinson et al., 2018; Santos et al., 2012).

Advective flow of seawater through sediments supplies benthic microbial communities with oxygen (O_2) and nitrate (NO_3^-), as well as particulate and dissolved organic matter, thus leading to high rates of organic matter degradation and nutrient turnover (Anschutz et al., 2009; Huettel & Rusch, 2000b; Kim et al., 2019). As such, coastal permeable sediments can contribute substantially to marine organic carbon remineralization, thereby affecting coastal nutrient and metal budgets (Huettel et al., 1998; Huettel et al., 2014; Van Raaphorst et al., 1990).

Organic matter degradation pathways in intertidal beach sediments may be restricted to aerobic respiration and NO_3^- reduction (Charbonnier et al., 2013) but can also include Mn and Fe reduction as well as sulfate reduction (McAllister et al., 2015). Rates of organic matter degradation coupled to aerobic respiration are usually high compared to other metabolisms (Froelich et al., 1979; Jørgensen & Sørensen, 1985) but are restricted to the layer where O_2 is available. This region is shaped by O_2 consumption and resupply and represents an important redox boundary with respect to nitrogen transformation and iron (Fe) and manganese (Mn) cycling (Froelich et al., 1979; Shaw et al., 1990).
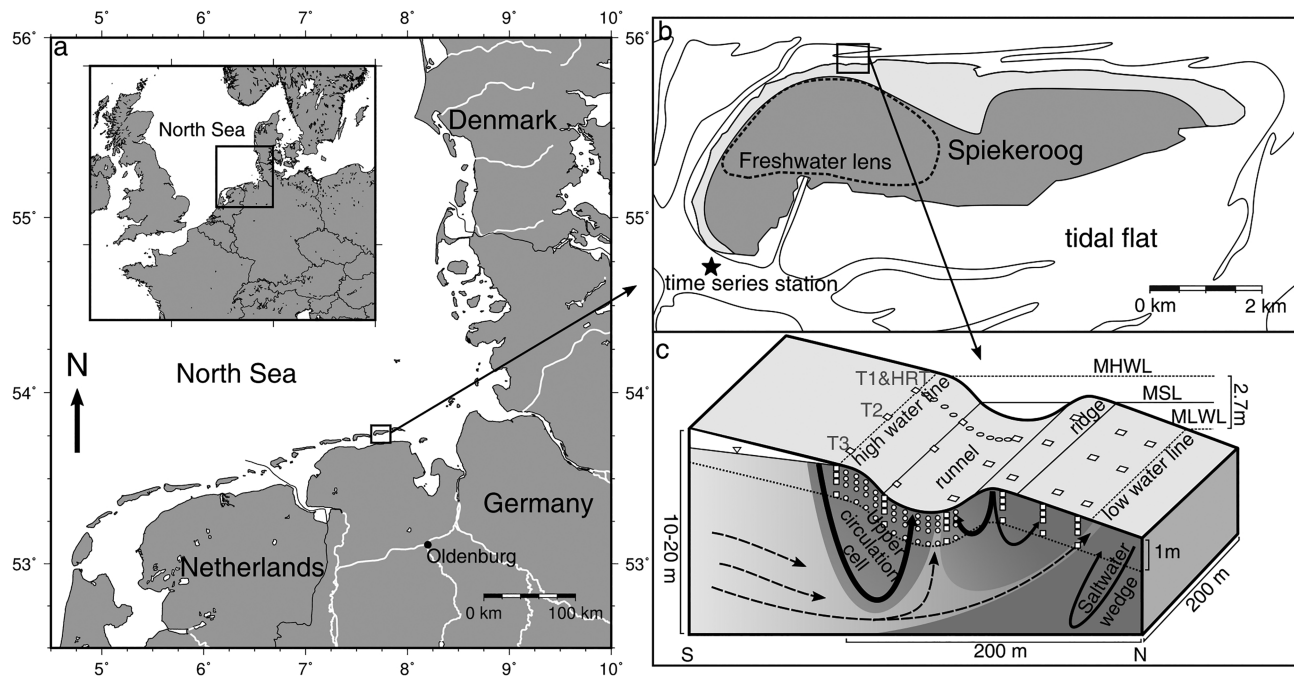
Nitrate reduction in subterranean estuaries can be driven by inputs of NO_3^- from fresh groundwater and inputs of marine organic matter (Couturier et al., 2017; Kim et al., 2017) as well as by seawater supplied NO_3^-. In combination with coupled nitrification-denitrification, the reduction of NO_3^- to nitrogen gas through denitrification can lead to substantial N-loss as N_2 and N_2O, which has been observed for permeable intertidal and subtidal sediments (Marchant et al., 2016; Marchant et al., 2018). The net removal of dissolved inorganic nitrogen (DIN) in beaches may therefore affect nutrient budgets in coastal regions where inputs of NO_3^- are high due to anthropogenic activities (Johannsen et al., 2008).

Further, intense Fe and Mn cycling has been observed in intertidal sediments (Beck et al., 2017; McAllister et al., 2015; O'Connor et al., 2015; Reckhardt et al., 2017; Roy et al., 2010). Pore waters can be enriched in these dissolved metals by orders of magnitude compared to seawater and thus form a potential source for coastal waters.

So far, the impact of pore water advection on biogeochemistry and pore water constituent effluxes from permeable sediments has mostly been studied in microtidal sheltered beaches (Beck et al., 2007; Gonneea & Charette, 2014; Liu et al., 2018; O'Connor et al., 2018; Santos et al., 2009), tidal flat areas (Beck et al., 2009; Billerbeck et al., 2006; Gao et al., 2012; Huettel & Rusch, 2000a; Marchant et al., 2014; Riedel et al., 2011), or subtidal sediments (Ahmerkamp et al., 2017; Marchant et al., 2016; Shum & Sundby, 1996), which are exposed to a lower wave energy level than high energy beaches. In contrast, only few studies have been conducted at wave exposed mesotidal to macrotidal sites like the French Aquitanian coast (Anschutz et al., 2009; Charbonnier et al., 2013; Charbonnier et al., 2016) or the beaches of Spiekeroog Island, Germany (Beck et al., 2017; Reckhardt et al., 2015; Seidel et al., 2015; Waska et al., 2019). In contrast to sheltered environments, chemical gradients in exposed sandy environments usually stretch over a larger depth range (McLachlan & Turner, 1994; Reckhardt et al., 2015). Thus, aerobic and nitrogen-driven respiration pathways contribute substantially to organic matter degradation and nutrient regeneration in high-energy environments (Charbonnier et al., 2013; Charbonnier et al., 2016; McLachlan, 1982).

Redox zonation and transformations in intertidal sediments vary not only in space but also in time. Seasonal variations in hydraulic head lead to changes in seawater residence times and magnitude of fresh groundwater input, which impact pore water geochemistry (Heiss et al., 2017; Michael et al., 2005). Similarly, across the year there are changes in organic matter composition and quantity as well as the quantity of nutrients and metals supplied from the water column (Kowalski et al., 2012; Meier et al., 2015; Seidel et al., 2015).

Combined, these seasonal variations may lead to changing distributions of subsurface redox species and nutrient transformation pathways (Santos et al., 2009; Charbonnier et al., 2013; Seidel et al., 2015; Charbonnier et al., 2016; O'Connor et al., 2018). The impact of seasonal variations on biogeochemistry in subterranean estuaries has mainly been assessed in microtidal sites with restricted wave exposure (Beck et al., 2007; Gonneea & Charette, 2014; Liu et al., 2018; O'Connor et al., 2018). Two studies addressing aerobic respiration on a French macrotidal exposed beach (Charbonnier et al., 2013; Charbonnier et al., 2016) revealed that seasonal drivers, including temperature and organic matter supply, control O_2 consumption and nutrient cycling.

Figure 1. Spiekeroog Island in the (a) southern North Sea and (b) north beach study area (black rectangle). The dashed line marks the freshwater lens extension according to Röper et al. (2012). The location of the time series station for pelagic water column sampling is indicated by a black star. The light grey colors in the northern part of Spiekeroog Island indicate primary dune distribution. Temporary exposed tidal flats are outlined by a black line. Subsurface sampling sites of transect samplings (□; T1 and T2 in October, March, and August and T3 in March) and high-resolution sampling (○; HRT in March and August) are shown in subfigure c. Conceptual hydrogeology, modified after Beck et al. (2017) and Waska et al. (2019), (solid arrows: seawater flow paths; dashed line arrows: freshwater flow paths) and sea level variations (MHWL: mean high water line; MSL: mean sea level; MLWL: mean low water line) are visualized.

The present study focuses on redox constituents in sediments influenced by mesotidal conditions at a high energy beach on Spiekeroog Island, Germany, located in the southern North Sea. Previous work at this site has indicated that the whole span of organic matter degradation pathways occurs, from aerobic respiration to sulfate reduction (Beck et al., 2017; Reckhardt et al., 2017; Waska et al., 2019).

In the comprehensive study by Beck et al. (2017), key processes, affecting beach pore water composition, were identified and subsurface biogeochemistry was linked to sedimentological, hydrogeological, and microbiological data. However, the spatial sampling resolution in the intertidal zone was low and sampling was conducted only once, in spring. Concurrently, samples from these sampling locations were analyzed for trace metals by Reckhardt et al. (2017). More recently, seasonal fluctuations in temperature, organic matter availability, and inland hydraulic head were identified as drivers for the seasonality in pore water concentrations of dissolved O_2 and reduced Fe (Waska et al., 2019). It was hypothesized that the general seasonal patterns are blurred due to continuous sediment redistribution occurring in the intertidal zone, which affects infiltration zones of seawater and exfiltration zones of pore waters. The conclusions were based on salinity, dissolved O_2, reduced Fe, and fluorescent organic matter analyses at 50 and 100 cm below surface. As benthic processes in intertidal sediments of Spiekeroog Island are linked to pelagic activity (Seidel et al., 2015), and geochemical data from intertidal pore waters indicate that seasonal effects play a role in determining benthic processes (Seidel et al., 2015; Waska et al., 2019), it is likely that seasonal variations may control electron acceptors and remineralization products and their transport across the sediment-water interface. Here, therefore, the following hypotheses were tested:

1. Advective pore water transport influences the succession of organic matter degradation processes in intertidal sands of a high energy beach by controlling the supply with seawater derived organic matter and electron acceptors.

2. Seasonal variations in coastal seawater composition affect benthic microbial activity and organic matter degradation pathways leading to seasonally changing spatial distributions of electron acceptors and remineralization products in shallow intertidal sands.

3. This seasonal variability in pore water biogeochemistry results in changing net fluxes across the sediment-water interface.

To assess these hypotheses, we monitored the pelagic water composition bimonthly and sampled the shallow intertidal pore waters in autumn, early spring, and summer. In detail, we studied dissolved O_2, DIN species (nitrite (NO_2^-), nitrate (NO_3^-), ammonium (NH_4^+)), dissolved Mn, and dissolved Fe. The spatial sampling resolution was increased within the intertidal zone, compared to previous studies, in order to distinguish spatial from temporal dynamics and to deduce microbial processes from pore water constituent distributions.

2. Materials and Methods

2.1. Study Site

The island of Spiekeroog is part of a barrier island chain located in the southern North Sea, NW Germany (Figure 1a). The sampling site is located on the north beach (Figure 1b). Based on a wave categorization scheme for this region, the near-shore significant wave height is 1.5 m (Dette, 1977). About 10–30 days exhibit storm conditions, annually (Antia, 1995). The site is influenced by mesotidal conditions with a mean tidal range of 2.7 m. During neap and spring tidal cycles, the tidal range changes to 2.4 and 3.3 m, respectively. The beach sediments of the upper meters are composed of fine to medium sand (mean grain size: 170–320 μm; Beck et al., 2017). The western part of the island is underlain by a freshwater lens (Figure 1b), which is confined by clay layer at about 40 m below NHN (standard elevation zero) and exhibits water ages up to 51 years (Röper et al., 2012; Seibert et al., 2018). Due to varying flow paths, fresh groundwater of various ages is delivered to the intertidal subsurface (Beck et al., 2017).
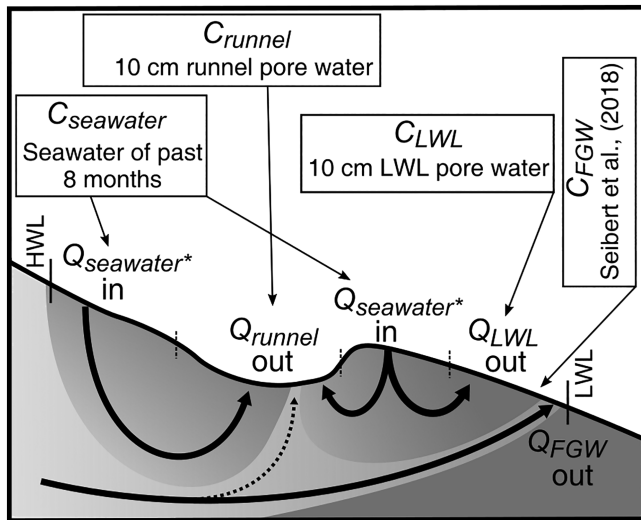
Spiekeroog beach exhibits morphological changes on different timescales, including erosional events like storm surges, sediment accumulation during calm conditions, and seasonal ridge migration. From spring to late autumn a pronounced ridge and runnel morphology evolves (Flemming & Davis, 1994; Waska et al., 2019).

According to a previously published hydrogeological model and high-resolution data of the intertidal area of the study site, the intertidal zone can be subdivided into two infiltration zones and two exfiltration zones (Figure 1c; Beck et al., 2017; Waska et al., 2019): Seawater infiltrates at the high water line (HWL) and discharges in the exfiltration zone in the runnel after weeks to months of residence time within the upper circulation cell. Concurrently, seawater infiltrates at the ridge and drains both landward and seaward. A mixture of upper circulation cell and ridge circulation pore water discharges in the runnel exfiltration zone, whereas ridge circulating pore water and potentially saltwater wedge water discharge at the exfiltration zone at low water line (LWL). Throughout the intertidal zone, but predominantly in low elevation areas, fresh groundwater mixes with circulating seawater, leading to locally restricted patches of brackish discharge (Waska et al., 2019).

2.2. Field Sampling

Samples were retrieved during three sampling campaigns in October 2016 (spring tide), March 2017 (neap tide), and August 2017 (spring tide). Six stations were sampled across coast-perpendicular transects extending from HWL to LWL (Figure 1c). Sampling was conducted around low tide in October and March and around high tide in August. The difference in tidal stage during sampling was unavoidable in order to meet the requirements of daylight, intertidal zone accessibility, and fair weather conditions. Additionally, a high-resolution transect was sampled in March and August ranging from the HWL to the landward slope of the ridge (Figure 1c). In August, the sampling strategy was further extended and pore waters were extracted using a grid pattern (~200 × 180 m; 192 samples; Waska et al., 2019). Pore water samples were collected at 10, 30, 50, and 100 cm below surface (cmbsf) along transects and at 50 and 100 cmbsf in the grid pattern. Stainless steel push-point samplers were used to sample pore waters. After extracting water with polyethylene syringes, dissolved O_2 was immediately determined using flow through cells and pocket oxygen meters (FireStingGO$_2$, Pyro-Science). In October, O_2 depth profiles were sampled on a parallel transect with 2-m distance from regular transect sampling. Oxygen probes were calibrated to 100% air-saturation using on-site seawater. The 0%

Figure 2. Conceptual hydrogeological model of infiltration and exfiltration zones (Beck et al. (2017), Waska et al. (2019)), as well as end-member selection for constituent flux calculations. Respective volumetric fluxes can be found in Table 1. *$Q_{seawater}$ balances the sum of Q_{runnel} and Q_{LWL}.

air saturation calibration solution was prepared by adding the strong reductant sodium dithionite (about 30 g/L) to that seawater sample. Using salinity and temperature data, the O_2 air-saturations were transformed into molar concentrations (Garcia & Gordon, 1992). Temperature and salinity were measured instantly using hand-held conductivity sensors (WTW). During each sampling campaign, discrete surficial seawater samples from the north beach of Spiekeroog were retrieved as well. Additionally, in 2016 and 2017 surficial seawater nutrient samples were taken bimonthly at the permanent time series station close to the western tip of Spiekeroog Island (Figure 1b). Furthermore, freshwater lens monitoring wells were sampled for metal analyses, according to sampling techniques described in Seibert et al. (2018).

To measure sulfide, approximately 1.5 ml of bubble-free extracted pore water was added to 0.6 ml 50 mM Zn acetate solution in preweighted Eppendorf vials.

Samples for NO_3^-, NO_2^-, and NH_4^+ analyses were filtered instantly using 0.45-μm surfactant-free cellulose acetate syringe filters, filled into high-density polyethylene vials, and poisoned with $HgCl_2$ yielding a 0.4 mM $HgCl_2$ solution.

Fe and Mn samples were filtered using 0.45-μm surfactant-free cellulose acetate syringe filters into low-density polyethylene bottles, which were acid-washed and rinsed with ultrapure water prior to use. After sampling, metal samples were acidified to 1% v/v using ultraclean concentrated HNO_3. Samples were stored cool and dark until analysis.

2.3. Laboratory Analyses

Nutrient samples were not stored longer than 6 days. NO_x^- and NO_2^- were measured photometrically using Griess reagent and vanadium(III) chloride as reduction agent (Schnetger & Lehners, 2014). For determining NH_4^+, a photometric method was adapted (Benesch & Mangelsdorf, 1972). Instead of phenol, we used sodium salicylate to prepare the catalyst reagent. Additionally, time series station surface water samples were analyzed for dissolved Si, applying a spectrophotometric method (Grasshoff et al., 1999). Replicate measurements of in-house reference solutions resulted in precisions of better than 7% (NH_4^+, NO_2^-), 4% (NO_x^-), and 9% (Si), respectively. The lowest calibration point was defined as limit of quantification. The limit of detection was therefore defined as one third of the limit of quantification (Table S9 in the supporting information). Dissolved sulfide was determined spectrophotometrically (Cline, 1969).

Trace metal samples from October were analyzed for Mn and Fe using sector field inductively coupled plasma mass spectrometry (SF-ICP-MS) with a resolution of $R = 4{,}500$ (Element 2, Thermo Fisher Scientific), whereas samples from March and August were analyzed using triple quadrupole ICP-MS (iCAP TQ ICP-MS, Thermo Fisher Scientific), applying the mode of kinetic energy discrimination to separate the analyte from polyatomic interferences. To measure within the calibration range, the samples were diluted with respect to their Mn and Fe concentration: All samples were diluted with 2% v/v HNO_3 of ultraclean grade at least tenfold and up to 100-fold for high Fe concentrations. Yttrium was used as an internal standard. To monitor trueness and precision, replicates of the two international standards Cass 5 and Nass 6 (National Research Council of Canada) were analyzed during each run. Aliquots of each reference material were spiked with Mn and Fe element standard solutions to concentrations of 0.46 μM Mn, respectively, 0.45 μM Fe as well as 0.91 μM Mn, respectively, 0.90 μM Fe, because pore water samples contained higher Mn and Fe concentration than both seawater reference standards. Replicate measurements of spiked reference standards yielded a trueness better than 2.9% and precision better than 2.6%. The limit of detection was calculated based on five to six blank replicates, which were measured during one run (Hubaux & Vos, 1970). It was multiplied with three to get the limit of quantification (Table S9).

2.4. Data Visualization

To suppress effects of vertical exaggeration during spatial interpolation, data points were interpolated on a rectangular grid with depth below surface on *y* axis. Afterward, these interpolated data were adjusted to

Table 1
Volumetric Fluxes of Infiltrating Seawater and Exfiltrating Pore Water Subdivided According to the Intertidal Zones (Beck et al., 2017)

[m³/day per m Shoreline]	Average	Range
Q_{runnel}	3.3	1.7–6.6
Q_{LWL}	1.0	0.5–2.0
Q_{FGW}	0.75	0.35–1.2[b]
$Q_{seawater}$[a]	4.3	2.2–8.6

[a]Sum of high water line and runnel infiltration. [b]Based on hydraulic gradient evaluations (Waska et al., 2019).

positions relative to standard elevation zero (NHN). The software package GMT 5 (Wessel et al., 2013) was used to compute and visualize the data.

2.5. Flux Calculations

Volumetric pore water fluxes to adjacent seawater were calculated for the study site by Beck et al. (2017), based on a numerical density-dependent groundwater flow and transport model. During its calibration, three model parameters (vertical and horizontal hydraulic conductivity and specific yield) were adjusted using groundwater levels measured in three groundwater wells located at supratidal and intertidal sites (Beck et al., 2017).

Infiltration zone (in) and exfiltration zone (out) boundaries within the model were operationally set by the half of surface elevation difference between (i) HWL and deepest runnel location, (ii) deepest runnel location and ridge top, and (iii) ridge top and LWL, respectively (Figure 2). The model provides time-averaged saline and fresh fluxes, which were calculated for distinct hydrogeological areas, representing main flow paths within the intertidal beach (Figure 2).

According to the model, seawater is delivered to the runnel exfiltration site from both HWL and ridge infiltration zones (Figure 2). On average, 2.8 m³/day per meter shoreline of seawater is infiltrating at HWL and 0.5 m³/day per meter shoreline is transported from ridge to runnel. In total, the resulting average saline runnel exfiltration Q_{runnel} is 3.3 m³/day per meter shoreline (Table 1). Further, from ridge to LWL an average saline flux Q_{LWL} of 1 m³/day per meter shoreline was derived from the model. The total saline efflux must therefore be balanced by a seawater volume influx $Q_{seawater}$ of 4.3 m³/day per meter shoreline. Based on groundwater recharge estimations, the average freshwater flux Q_{FGW} was assigned to be 0.75 m³/day per meter shoreline on average (Table 1).

The overall error on saline volumetric fluxes has been assumed to range from 0.5 to 2 times the average fluxes (Table 1; Beck et al., 2017). The halving of saline fluxes was assigned to the overestimation of ridge infiltration rates by the model (Beck et al., 2017). This overestimation not only led to uncertainty in fluxes but has also been identified to highly affect fresh groundwater flow paths:

The model from Beck et al. (2017) revealed that fresh groundwater discharges in a restricted zone within the low lying runnel. In contrast, subsequent salinity mapping and additional hydraulic head measurements of the intertidal zone indicated that fresh groundwater discharges at LWL, too (Figures 1c and 2; Waska et al., 2019). The one fresh groundwater discharge tube concept was attributed to ridge head overestimations in the Beck et al. (2017) model. It produced a nonexistent groundwater divide preventing fresh groundwater from discharging at the LWL and further demonstrated the sensitivity of the flow path system to ridge morphology changes, which occur frequently in the study area (Waska et al., 2019). The fresh groundwater flux is assumed to be unaffected by its flow path through the intertidal beach.

The Beck et al. (2017) model did not account for wave forcing and storm floods. Therefore, the factor 2 has been assigned to saline volumetric fluxes to define the positive error range. Based on a numerical study on effects of tidal and wave forcing on a subterranean estuary, the doubling of saline seawater circulation rates could have been observed by adding wave forcing to a tidal model (Xin et al., 2010).
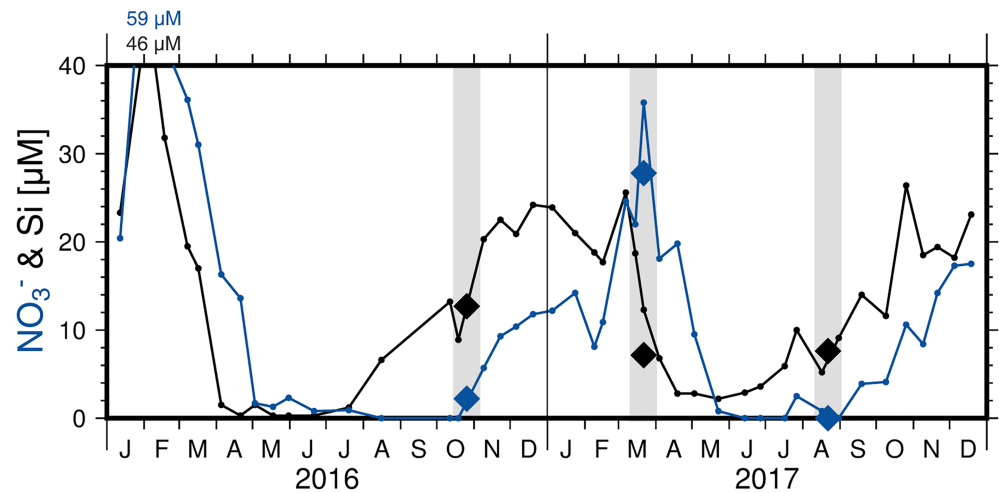
The intraannual variation of the fresh groundwater flux was estimated from seasonal hydraulic gradient changes along the flow paths from the groundwater divide at the center of the island toward the beach, and ranged from 0.35 to 1.2 m³/day per meter shoreline (Table 1; Waska et al., 2019).

To calculate constituent fluxes to the coastal waters, pore water and seawater end-member concentrations were multiplied with volumetric fluxes and summed up to get total efflux J_{out}, influx J_{in}, and net flux J_{net}:

$$J_{out} = Q_{runnel} \cdot C_{runnel} + Q_{LWL} \cdot C_{LWL} + Q_{FGW} \cdot C_{FGW}$$

$$J_{in} = Q_{seawater} \cdot C_{seawater}$$

$$J_{net} = J_{out} - J_{in}$$

Figure 3. Seasonal variations of dissolved NO_3^- (blue) and silica (black) in the water column at a nearby time series station in the tidal inlet between Spiekeroog and Langeoog Island. Samples taken in the water column at the north beach during pore water sampling campaigns on Spiekeroog Island are marked with a diamond symbol. The grey shaded areas represent beach sampling campaigns. Concentrations above 40 μM are indicated by their respective concentration (NO_3^-: blue and silica: black).
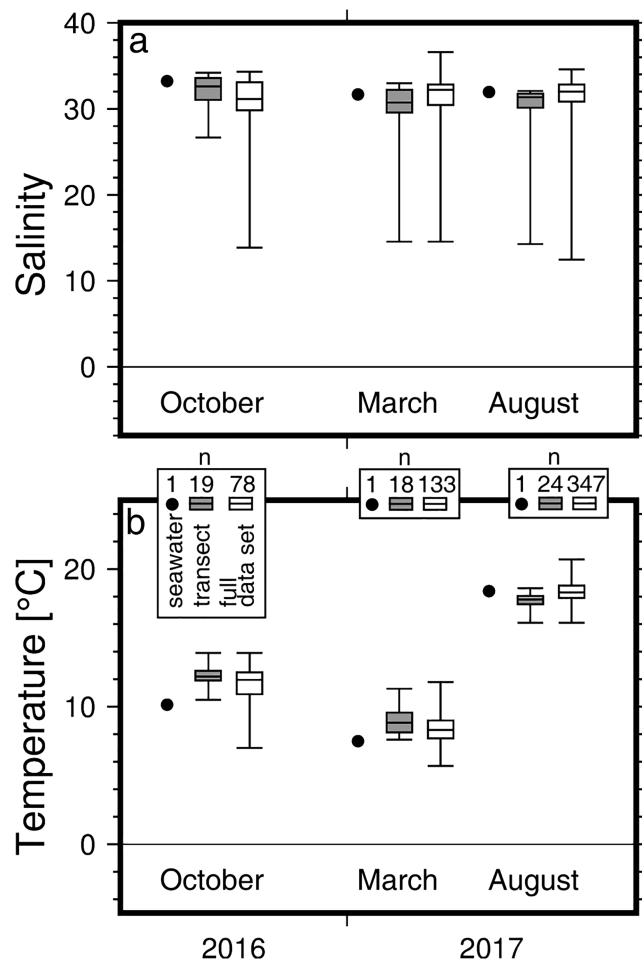
Saline volumetric fluxes were multiplied with pore water end-members from intertidal sites. The saline end-member concentrations C_{runnel} and C_{LWL} were chosen among 10-cmbsf samples from runnel and LWL of transect T1 and HRT (Figure 2; salinity >26; O_2 <10 μM). Recent seawater as well as time averages of past seawater compositions up to 8 months were defined as seawater end-members $C_{seawater}$ (Tables S6–S8). Eight months corresponds to the maximum seawater residence time in the upper circulation cell (Beck et al., 2017). Fresh groundwater volumetric fluxes, in contrast, were multiplied with an averaged inland fresh groundwater composition to take into account the uncertainties in fresh groundwater flow paths (Waska et al., 2019) and the small number of brackish beach pore water end-members. Fresh groundwater end-member concentrations C_{FGW} were averaged from inland monitoring wells for nutrient (Seibert et al., 2018) as well as Mn and Fe data (Tables S6–S8).

Owing to the large range in possible residence times as well as in pore water end-member concentration, individual constituent fluxes for any combination of seawater age (from zero to eight months) and available pore water end-members were calculated. To consider as well the volumetric flux uncertainty, the average, minimum, and maximum fluxes (Table 1) were used for constituent flux calculations. The resulting individual fluxes were summarized in boxplots. In the following, "fluxes" refer to median fluxes.The applied model assumes that the end-members C_{runnel} and C_{LWL} are representative for exfiltration areas. However, the LWL sampling sites were operationally defined by the lowest reachable saline site (salinity >26) and any subtidal exfiltration areas, which may be connected to intertidal infiltration zones, receive no consideration. The model assumes that the volumetric fluxes remain constant throughout the year.

3. Results

3.1. Surface Water

NO_3^- concentrations in north beach seawater were 3 and 28 μM in October and March, respectively, and below detection limit in August. NO_3^- concentrations from the nearby time series station showed a high variability throughout the year (Figure 3). Highest NO_3^- concentrations were found from January to March. The maximum of 59 μM was measured in February 2016. From April to May these concentrations decreased sharply down to below detection limit and remained low until September. Afterward, NO_3^- concentrations increased again. Seawater Si data exhibited the same seasonal pattern as NO_3^- except that the sharp decline down to values below detection limit was observed about 1 month earlier. Seawater NO_2^-

Figure 4. Seasonal variations of (a) salinity and (b) temperature, shown for the transect subset (grey) and for all samples (white). Shown are minimum, 25th percentile; median, 75th percentile; and maximum values. The black dots () represent north beach seawater. Sample size n can be found in the small boxes.

from north beach was below detection limit, except for March (0.8 μM). The highest NH_4^+ concentration was found in north beach seawater in October (9 μM), whereas NH_4^+ was either at detection limit in March, or below limit of quantification in August (<5.8 μM; Figure 7). Seawater Mn concentrations at the north beach were below 0.1 μM and thus very low in comparison with obtained pore water concentrations (Figure 6). Similar to Mn, north beach seawater Fe concentrations (<0.03 μM) were orders of magnitude lower than pore water concentrations.

3.2. Pore Water
3.2.1. Salinity and Temperature
Although pore water salinities ranged from 12.5 (brackish) to 36.6 (saline), the median salinity of all samples was at 32.0 and 75% of all samples exhibited salinities above 30.6 (Figure 4a). Confirming the results of Waska et al. (2019), we found brackish discharge patches throughout the intertidal zone especially at the LWL, but also at runnel sites (supporting information, Figures S1, S5, and S6). North beach seawater salinity ranged from 31.6 to 33.2.

Pore water temperatures changed seasonally, with almost no overlap in the temperature ranges between the sampling campaigns. Corresponding seawater temperatures were below median pore water temperatures in October and March, and above in August (Figure 4b).

3.2.2. O_2 and Sulfide
The highest pore water O_2 concentrations corresponded to concurrent north beach seawater concentrations for October and March campaigns (285 μM in October and 307 μM in March; Figure 5a). In August, the maximum concentration of all samples (200 μM) was notably lower than the corresponding seawater concentration (245 μM) and 75% of the samples contained O_2 concentrations of less than 20 μM (Figure 5a).

In general, dissolved O_2 was found in highest concentrations close to the HWL and gradually decreased toward the runnel and with depth (Figures 6, S5, and S6). O_2 was elevated on the top of the ridge, depending on season. Close to the LWL, O_2 was absent at all sampling depths. In October and March, the O_2 penetration depth ranged from deeper than 100 cmbsf at the HWL to les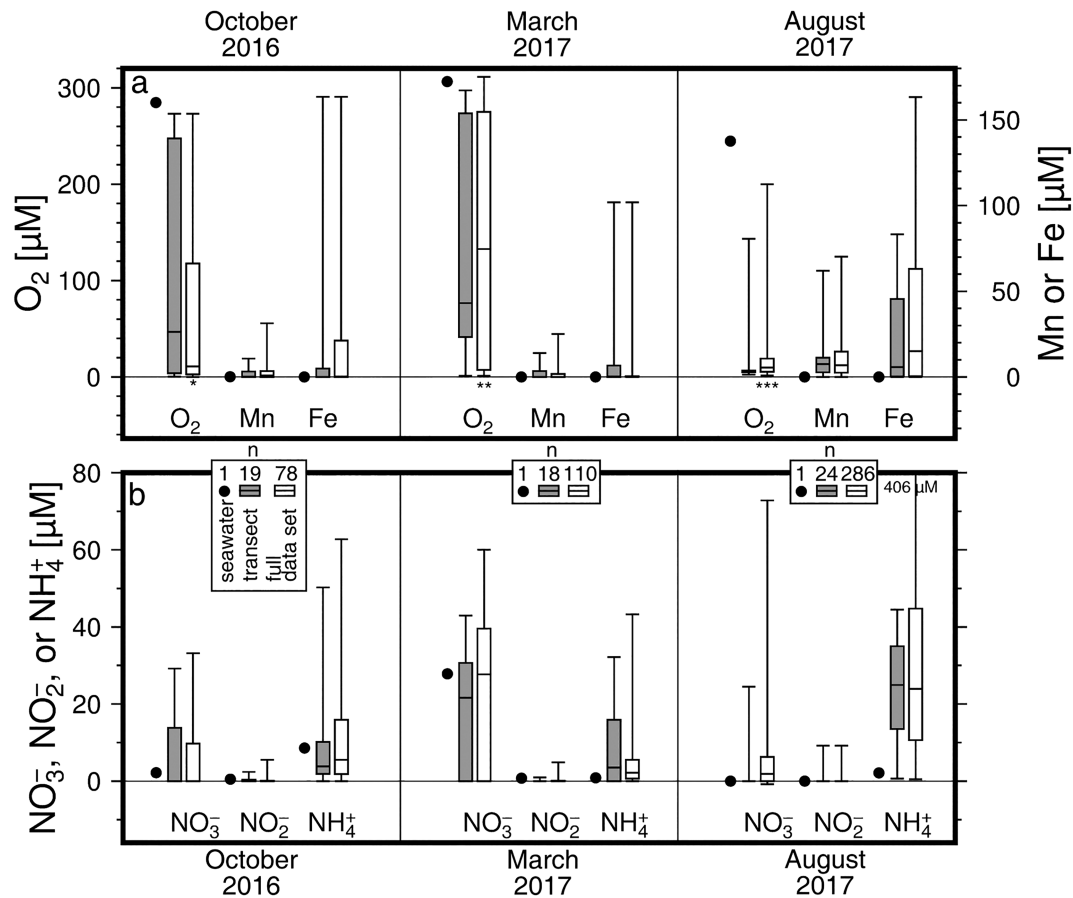s than 10 cmbsf at the LWL or at runnel sites (Figures 6, S5, and S6). A sharp horizontal gradient was observed at 35-m distance to the HWL in March, which was mapped precisely by the high-resolution sampling (Figure 6b). In contrast to October and March, O_2 was restricted to the upper beach close to the HWL in August and no O_2 was detected at the ridge. Furthermore, O_2 penetration depth was much lower.

Dissolved sulfide was either close to or below the limit of quantification (5 μM) in all samples (data not shown). However, we found indications of sulfate reduction. In some pore water samples from the LWL or from the runnel, sulfide smell was recognized.

3.2.3. Nitrate, Nitrite, and Ammonium
Within the pore waters, NO_3^- concentrations ranged between 0 and 73 μM over all seasons. The median of the March samples (22 μM) exceeded those of October and August (both below detection limit; Figure 5b). Spatial NO_3^- patterns were similar in all seasons with highest concentrations at elevated parts of the beach, that is, HWL and ridge. Concentrations at these sites exceeded concurrent seawater NO_3^- in many samples. At the LWL and in runnel sediments, NO_3^- was absent (Figures 7, S7, and S8). Generally, spatial NO_3^- patterns were similar to the O_2 distribution (Figures 6, 7, S5, S6, S7, and S8), except for March when high NO_3^- concentrations could still be found at the ridge, where O_2 was already depleted. In contrast to October and March, NO_3^- was only detected at the HWL in August.
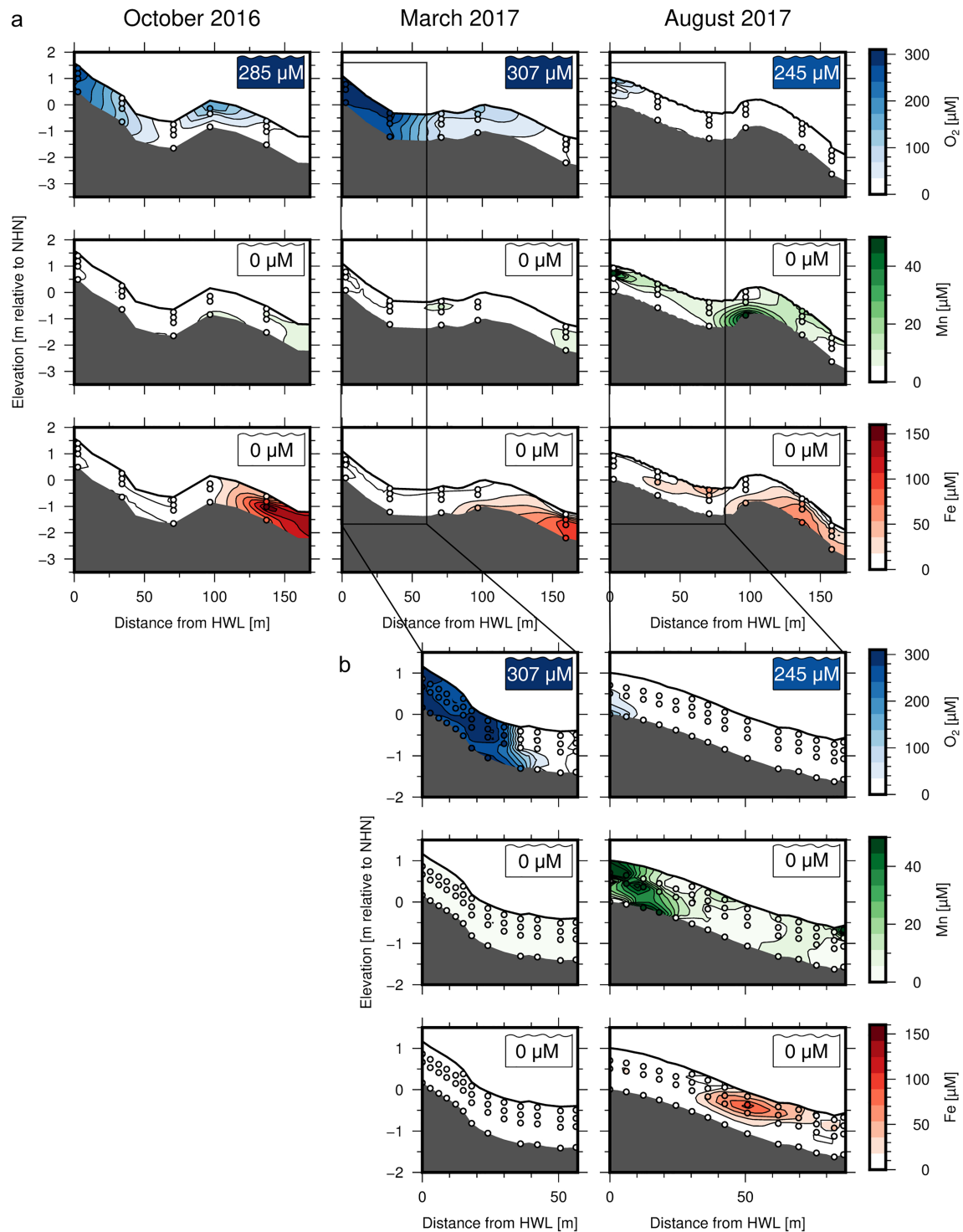
Figure 5. (a) Seasonal variations of oxygen (O_2), manganese (Mn), and iron (Fe) in pore waters, as well as of nitrate (NO_3^-), nitrite (NO_2^-), and ammonium (NH_4^+). (b) Minimum, 25th percentile; median, 75th percentile; and maximum of transect subset (grey) and full data set (white). The black dots () represent north beach seawater. Sample size n can be found in the small boxes. O_2 sample sizes deviate from overall sample size: *55 samples in March, **133 samples in March, **347 samples in August.

NO_2^- was only found at some spots with concentrations generally below 1 μM. Elevated NO_2^- was generally found at depths below high NO_3^- concentrations. Concurrently, in these samples NO_3^- was depleted compared to adjacent sampling depths (Figures S2, S7, and S8).

Overall NH_4^+ concentrations ranged from 0 to 163 μM, excluding one sample from August (406 μM). Although the entire concentration range was different, October and March transect samples exhibited comparable median (both at 4 μM) and upper quartile concentrations (10 and 16 μM, respectively). In contrast, both median (25 μM) and upper quartile (35 μM) were higher in August (Figure 5b). In October and March, NH_4^+ was restricted to the LWL and runnel. In contrast, NH_4^+ was present nearly throughout the whole intertidal zone in August with only few exceptions (Figures 7, S7, and S8).
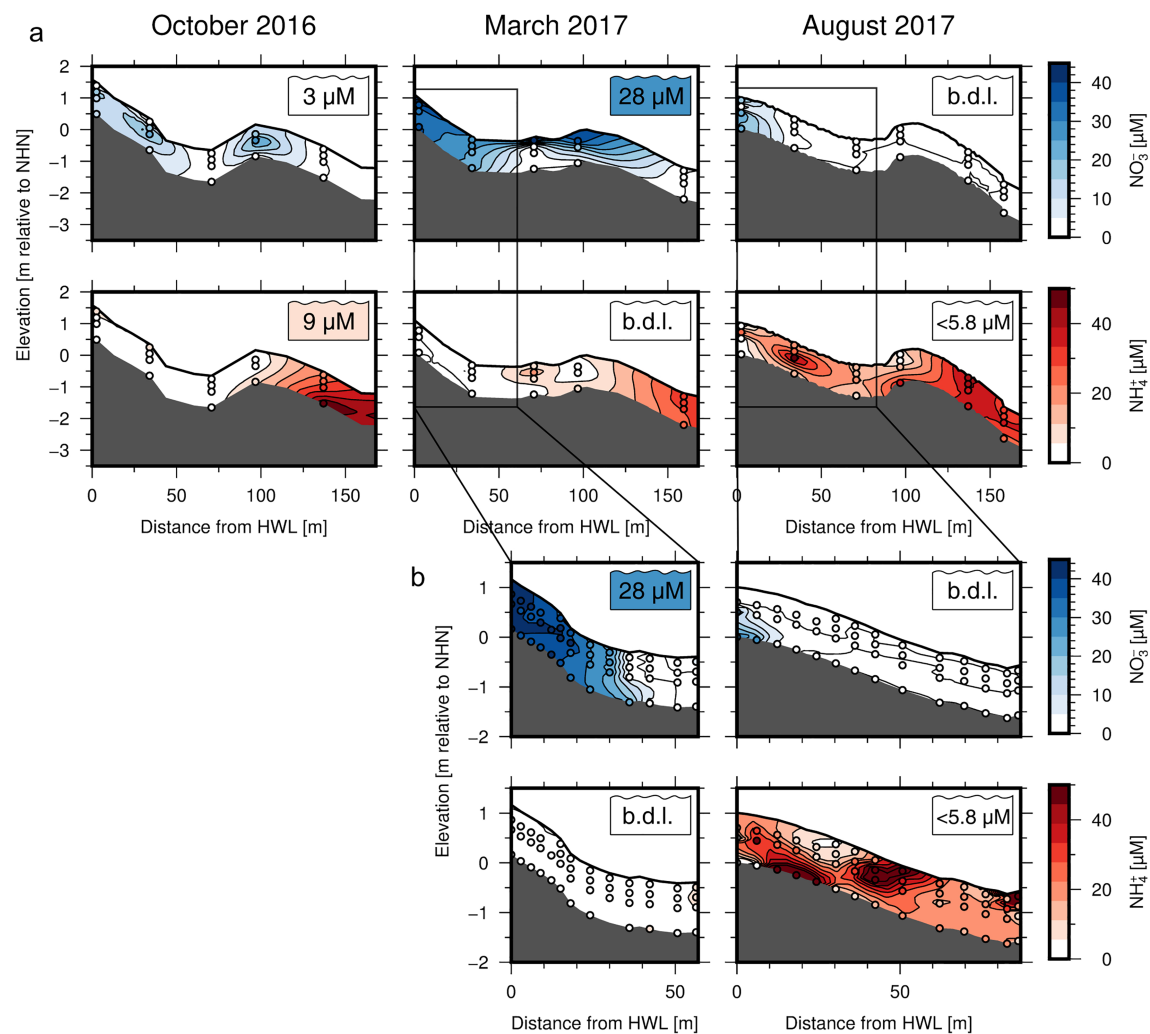
3.2.4. Dissolved Manganese and Iron

Dissolved Mn was detected in most samples at concentrations <20 μM; however, concentrations reached up to 70 μM (Figure 5a). During all campaigns, elevated concentrations were found in ridge pore waters and close to the LWL (Figures 6, S5, and S6). In March, dissolved Mn was additionally detected in the runnel (14 μM). In August, Mn concentrations were highest compared to the other seasons (Figure 5a) and Mn was patchy distributed across the entire subsurface of the intertidal zone (Figures 6, S5, and S6). Dissolved Fe concentrations ranged up to 163 μM (Figure 5a), and highest concentrations were predominantly found close to the LWL (Figures 6, S5, and S6). The highest Fe concentrations were found in October (up to 163 μM). In general, lower concentrations were observed in March (<102 μM), but

Figure 6. Pore water oxygen (O_2), manganese (Mn) and iron (Fe) (a) for October, March, and August measured in low resolution in the entire intertidal zone and (b) for March and August in higher resolution from high water line to runnel. Corresponding seawater concentrations can be found in the top right color-coded boxes.

the spatial distribution was similar to October (Figure 6). In August, dissolved Fe was spatially more heterogeneously distributed and also found at higher elevation levels across the beach face slope to the runnel as well as in the runnel (Figure 6).
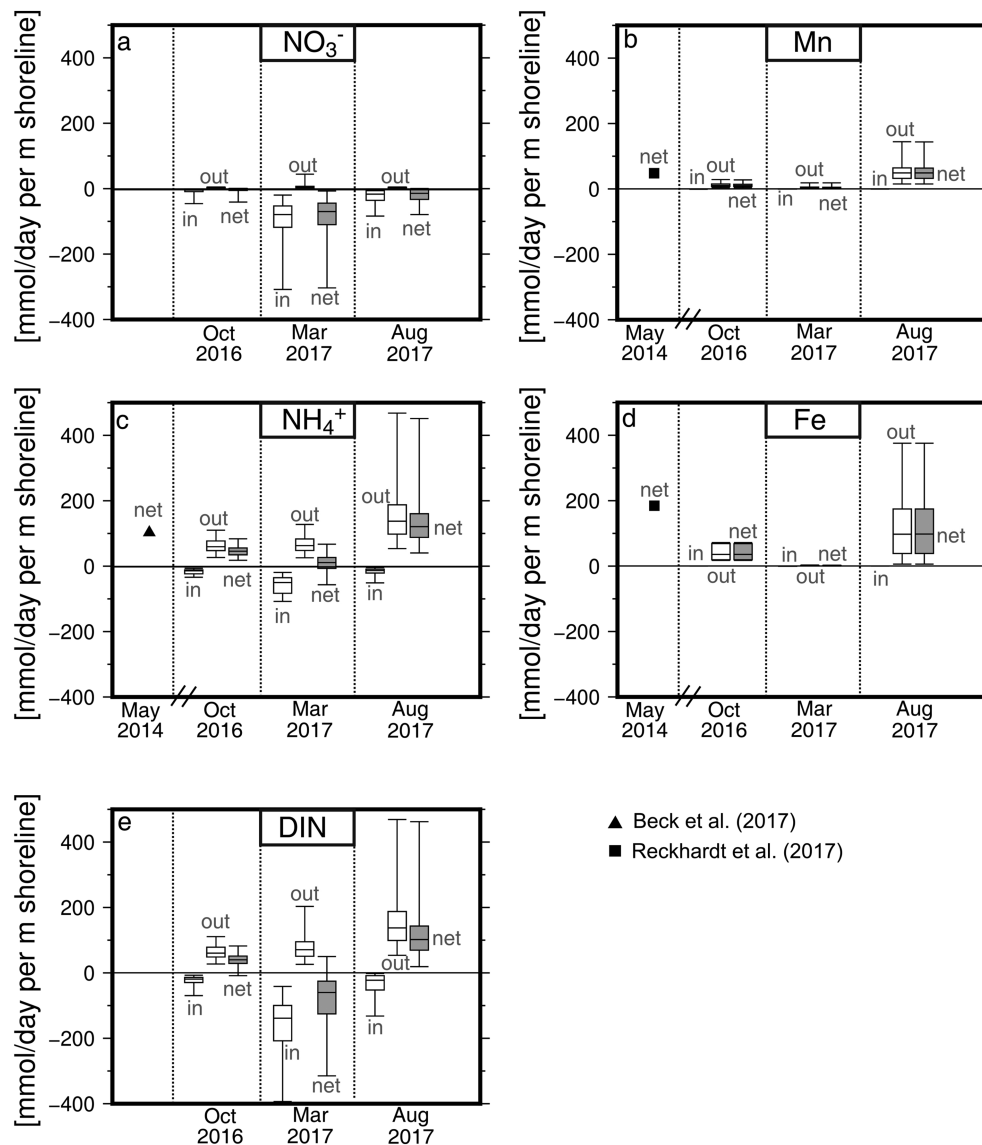
Figure 7. Pore water nitrate (NO_3^-) and ammonium (NH_4^+) for October, March, and August measured along the transect (a) and for March and August in higher resolution (b). Corresponding seawater concentrations can be found in the top right color-coded boxes."b.d.l.": values below detection limit.

3.3. Fluxes

The NO_3^- net flux to surface waters was negative throughout the year. From October (−1 mmol NO_3^-/day per meter shoreline) to March (−70 mmol NO_3^-/day per meter shoreline) NO_3^- net removal from seawater increased but decreased again toward August (−14 mmol NO_3^-/day per meter shoreline; Figure 8a). The negative net flux was caused by continuous influx of NO_3^- into intertidal sediments (−4 to −79 mmol NO_3^-/day per meter shoreline). The efflux remained below 4 mmol NO_3^-/day per meter shoreline in all campaigns.

The NH_4^+ net flux in August (121 mmol NH_4^+/day per meter shoreline) was up to 1 order of magnitude higher compared to October and March (46 and 11 mmol NH_4^+/day per meter shoreline, respectively) and in the same order as the NH_4^+ net flux calculated by Beck et al. (2017; 117 mmol NH_4^+/day per meter shoreline; Figure 8c). Generally, influxes were lower than effluxes, causing positive net fluxes throughout the year.

DIN net fluxes (sum of NO_3^-, NO_2^-, and NH_4^+) exhibited a change from a DIN source (positive net flux) in October to a DIN sink (negative net flux) in March (40 and −60 mmol DIN/day per meter shoreline, respectively). In August the DIN net flux was highest (102 mmol DIN/day per meter shoreline; Figure 8e).
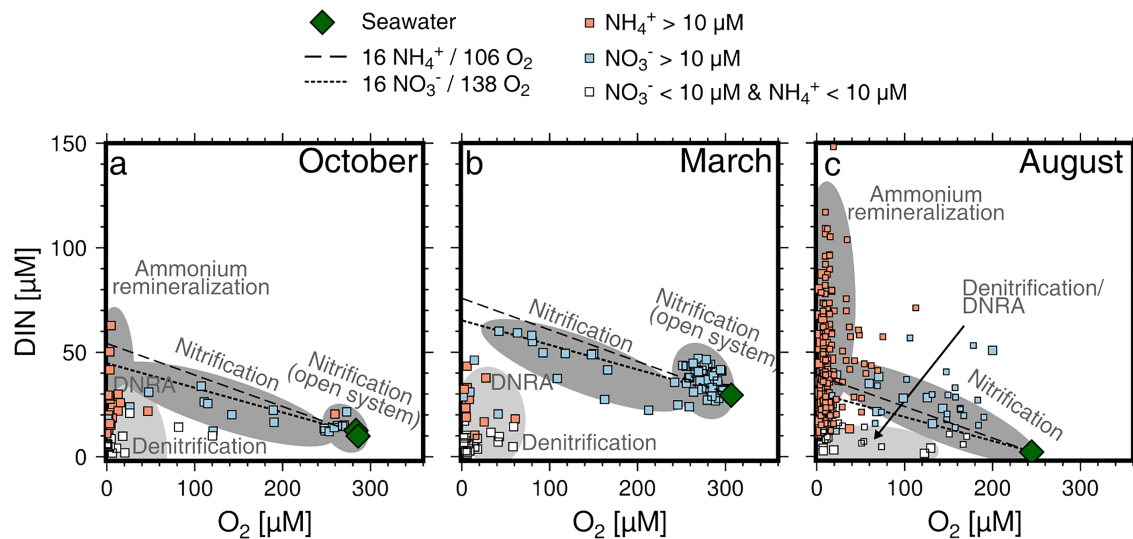
Figure 8. Seasonal variability of potential (a) NO_3^-, (c) NH_4^+, (e) DIN, (b) Mn, and (d) Fe fluxes to nearshore waters. Fluxes are divided into influx (in), efflux (out), and net flux (sum of influx and efflux; net) and are shown in boxplots. Negative fluxes refer to a transport into the beach sediments. For May 2014 only net fluxes were available for NH_4^+, Mn, and Fe (Beck et al., 2017; Reckhardt et al., 2017). The error bars derive from temporal seawater end-member variability (in), spatial heterogeneity in runnel and low water line (LWL) samples (out), and volumetric flux variability.

August dissolved Mn net flux (49 mmol Mn/day per meter shoreline) was about 4 times higher than both October and March fluxes (10 and 4 mmol Mn/day per meter shoreline, respectively; Figure 8b). The dissolved Mn net flux in August was comparable to the dissolved Mn flux calculated for May 2014 (48 mmol Mn/day per meter shoreline) based on 50 cmbsf end-members by Reckhardt et al. (2017; Figure 8b). Due to low influxes, net fluxes were mainly governed by effluxes.

Dissolved Fe net fluxes decreased from October (36 mmol Fe/day per meter shoreline) to March (2 mmol Fe/day per meter shoreline) and increased to a maximum flux in August (98 mmol Fe/day per meter shoreline). The dissolved Fe net flux calculated by Reckhardt et al. (2017) for the same site in May 2014 (185 mmol Fe/day per meter shoreline) is higher than the interquartile range of dissolved Fe net fluxes calculated for August 2017 in this study (32–144 mmol Fe/day per meter shoreline). Analogous to Mn, the influx of dissolved Fe was negligible (Figure 8d).

Figure 9. Dissolved inorganic nitrogen (DIN) as function of dissolved oxygen (O_2) for (a) October, (b) March, and (c) August. Symbols are filled according to the concentration of the present DIN species (nitrate (NO_3^-): blue colors; ammonium (NH_4^+): red colors*). Stoichiometric NH_4^+ release per consumed O_2 molecule is shown, assuming Redfield stoichiometry (16:106) for aerobic respiration (dashed line). Further O_2 uptake by NH_4^+ oxidation to NO_3^- ($NH_4^+ + 2O_2$ $NO_3^- + H_2O + 2H^+$) results in an overall ratio of 16 NO_3^- to 138 O_2 (dotted line). Nitrogen transformations were identified according to DIN species concentrations and their relation to the theoretical release curve. Samples, which plotted around the release curves, mostly containing NO_3^-, are assumed to result from coupled aerobic respiration and subsequent nitrification. Positive deviations (excess NO_3^-) reveal that seawater continuously delivers O_2, for example, due to open system conditions at high water line. Negative deviations and low DIN concentrations below seawater NO_3^- are considered to result from denitrification/ dissimilatory nitrate reduction to ammonium (DNRA), whereas high NH_4^+ concentrations are thought to be caused by ammonium remineralization, i.e., during Mn and Fe reduction. * including a few samples containing both NH_4^+ and NO_3^- above 10 μM.

4. Discussion

4.1. Pore Water Biogeochemistry

4.1.1. General Patterns in Flow Paths and Redox Zonation

Generally, flow paths within beaches, in particular, infiltration and exfiltration zones, determine seawater constituent supply (O_2, NO_3^-, and marine organic matter) and the discharge of remineralization products (Mn, Fe, and NH_4^+). At our study site, the pore water salinity corresponded with that of the seawater, indicating that seawater circulation was the predominant driver of intertidal pore water geochemistry. This is in line with previous studies at the site (Beck et al., 2017).

While O_2 penetrated deeply into the sediment at infiltration zones on the beach, it barely penetrated into the sediment in exfiltration zones, regardless of whether pore waters were saline or brackish. This led to a sharp vertical O_2 boundary located between HWL and runnel at the border of the infiltration and exfiltration zones (Figure 6b). O_2 dynamics were driven by microbial consumption and were closely correlated to N-species: NO_3^- concentrations were consistently elevated in oxic parts of the sediment and were often higher than those in the overlying water. This suggests that remineralized NH_4^+ is nitrified to NO_3^- in these zones (Figures 7 and 9). Below oxygenated sediments, NO_3^- was depleted and was likely transformed to NH_4^+ via dissimilatory nitrate reduction to ammonium (DNRA), to gaseous N_2/N_2O via denitrification, or consumed by microorganisms within the sediments. Consequently, there were zones in the sediment where pore waters had low DIN and low O_2 (Figures 7, 9, and S3). A similar coupling of nitrification and denitrification has been found in intertidal sands from Tolo Harbor, Hongkong (Liu et al., 2017) and in nearby subtidal sediments of the North Sea where N-loss is high. In these permeable sediments, denitrification appears to be favored over anammox due to high organic matter input and rapid fluctuations in O_2 concentrations (Marchant et al., 2016; Marchant et al., 2017).

Additional NH_4^+ was delivered to brackish mixing zones by fresh groundwater from the inland's freshwater lens, which carries up to 78 μM NH_4^+ (Seibert et al., 2018), but highest NH_4^+ concentrations were found in saline anoxic pore waters and most likely produced in situ during anaerobic respiration (Figure S4). Due to the cooccurrence with reduced substances like dissolved Fe and Mn (Figures 6 and 7), it is likely that NH_4^+

was released during organic matter degradation via Mn or Fe oxide reduction and is not subject to rapid (re-) oxidation in these environments.

Dissolved Mn and Fe are produced, when particulate Mn and Fe minerals are reduced during organic matter degradation, which occurs after the complete consumption of more favorable electron acceptors like O_2 or NO_3^- (Beck et al., 2017). This general pattern was found in our study as well, indicated by the occurrence of Mn and Fe concentrations in zones of O_2 depletion. Mn and Fe concentrations are expected to be highest in exfiltration zones. However, in shallow pore waters of exfiltrating sites (10 cmbsf), we found depletions of Mn and Fe compared to deeper layers, probably due to potential oxidation of both compounds. In intertidal sediments the oxidation of dissolved Mn and Fe by O_2 and NO_3^- is a likely process due to advective pore water transport (Caetano et al., 1997; Luther et al., 1997). Concurrently, dissolved Fe may form solid Fe sulfides, when it reacts with dissolved sulfide (McAllister et al., 2015). Although, Fe-S-interactions are present at the studied sediment depths (<100 cmbsf), they are of less importance as these sediments at the study site are generally characterized by low rates of bacterial sulfate reduction and sulfide reoxidation (Reckhardt et al., 2017).

4.1.2. Seasonal Trends in Pore Water Geochemistry

Although the same general geochemical zonation was observed during all three sampling campaigns, substantial seasonal changes occurred. The O_2 penetration depth as well as the spatial distribution of NO_3^- and reduced metabolites, like NH_4^+, Mn, and Fe, varied seasonally (Figures 6 and 7). A changing O_2 penetration depth is an essential factor for biogeochemical processes, because it separates aerobic from anaerobic respiration pathways. O_2 and NO_3^- are the most favorable electron acceptors (Froelich et al., 1979), and their availability mostly suppresses the utilization of other electron acceptors with lower energy yield.

In October and March, deep O_2 penetration and excess NO_3^- indicated aerobic respiration to be the most prominent organic matter degradation pathway in shallow sediments. Concurrently, the runnel site seemed to be a hotspot of DIN-loss where pore waters were found to be low in O_2, DIN, Mn, and Fe (Figure 6, 7, and S3). Indications for Mn and Fe reduction co-occurred with highest loads of NH_4^+ but were restricted to the LWL.

In contrast to October and March, dissolved O_2 was restricted to the uppermost sampling depths in August, which indicated an increased O_2 consumption rate at that time (see also Waska et al., 2019). There was no pronounced DIN minimum in August (Figures 7 and S3), which does not necessarily mean that denitrification was absent, but intensified remineralization releasing NH_4^+ caused excess DIN (Figure 9). Simultaneously, indications for Mn and Fe reduction were found throughout the intertidal subsurface, including upper beach sites and runnel locations.

The sampling in August was conducted during a different tidal state (shortly after high tide) compared to those in March and October (after low tide). Therefore, we cannot completely rule out an imprint of tidal dynamics on our results, for example, on dissolved O_2. In August, oxygenated seawater was introduced into the sediment shortly before sampling. This could have increased dissolved O_2 concentrations at HWL locations (Charbonnier et al., 2016) compared to samplings at the same sites during rising tides. Thus, seasonal dynamics would have been rather underestimated than overestimated. Further, tidal dynamics have been shown to even affect pore waters down to 3 mbsf. The observed tidal changes in DIN species were in the range of lower μM, and the overall species distributions did not change significantly (Liu et al., 2017). We cannot exclude that tidal variabilities might have overprinted our results. Nevertheless, we think that the magnitude of the seasonal variability is much higher than that of tidal dynamics.

4.1.3. Pelagic Organic Matter Availability Affects Benthic Rates

O_2 penetration depth is a result of O_2 uptake rates, and transport rates. Assuming no drastic changes in the latter, the mainly microbially mediated O_2 uptake rates are assumed to vary highly with season. Increases in O_2 uptake rates would reduce the O_2 penetration depth, thereby promoting anaerobic degradation pathways in shallow sediments.

Benthic organic matter degradation rates respond to changes in organic matter composition and quantity. Fresh marine-derived organic matter is predominantly available from late spring to early autumn due to

intense pelagic activity in our study area (Meier et al., 2015; Seidel et al., 2015). Labile organic matter stimulates benthic carbon degradation and enhances microbial rates (Hedges et al., 1988).

The seasonal changes in primary production in the Wadden Sea area are reflected in Si and NO_3^- concentrations determined in the open water column at a nearby permanently installed time series station (Beck & Brumsack, 2012; Grunwald et al., 2010). Silica decreases in spring are linked to diatom frustule production. Spring Si and NO_3^- decreases are caused predominantly by uptake, but concentrations are also affected by sedimentary recycling processes in sediments and water column (Grunwald et al., 2010). Further NO_3^- inputs from rivers vary seasonally (Johannsen et al., 2008).

Based on nutrient concentrations measured in the water column in 2016 and 2017 (Figure 3), it can be deduced that the March sampling campaign took place during starting bloom conditions, because Si concentrations were already declining. Therefore, we expect a rather low supply of labile marine organic matter in March. Consequently, aerobic respiration rates were assumed to be comparably low, allowing O_2 to penetrate deep (>1 mbsf) into the sediment (Figure 6).

In contrast, the August campaign took place during postbloom conditions, when most nutrients of the coastal water inventory were depleted (Figure 3). The preceding bloom would have resulted in an enhanced supply of labile organic matter to beach sediments in the months and weeks before. This leads to the complete O_2 consumption in shallow sediment depths and consequently to the shift to other electron acceptors like solid Mn and Fe oxides (Figure 6). During the October campaign, water column nutrient remineralization exceeded nutrient consumption. Based on pore water O_2 and NO_3^- distributions (Figures 6 and 7), we expect October to be an intermediate state between March and August with respect to labile organic matter availability and O_2 consumption rates.

The supply of labile organic matter is not only related to current pelagic activity. Due to its reduced mobility, particulate organic matter is further trapped in intertidal sediments. This "carbon memory" has been observed to enhance microbial rates for up to 2 months (Kim et al., 2019). It is thus likely that both August and October rates have been affected by the high pelagic activity in prior months.
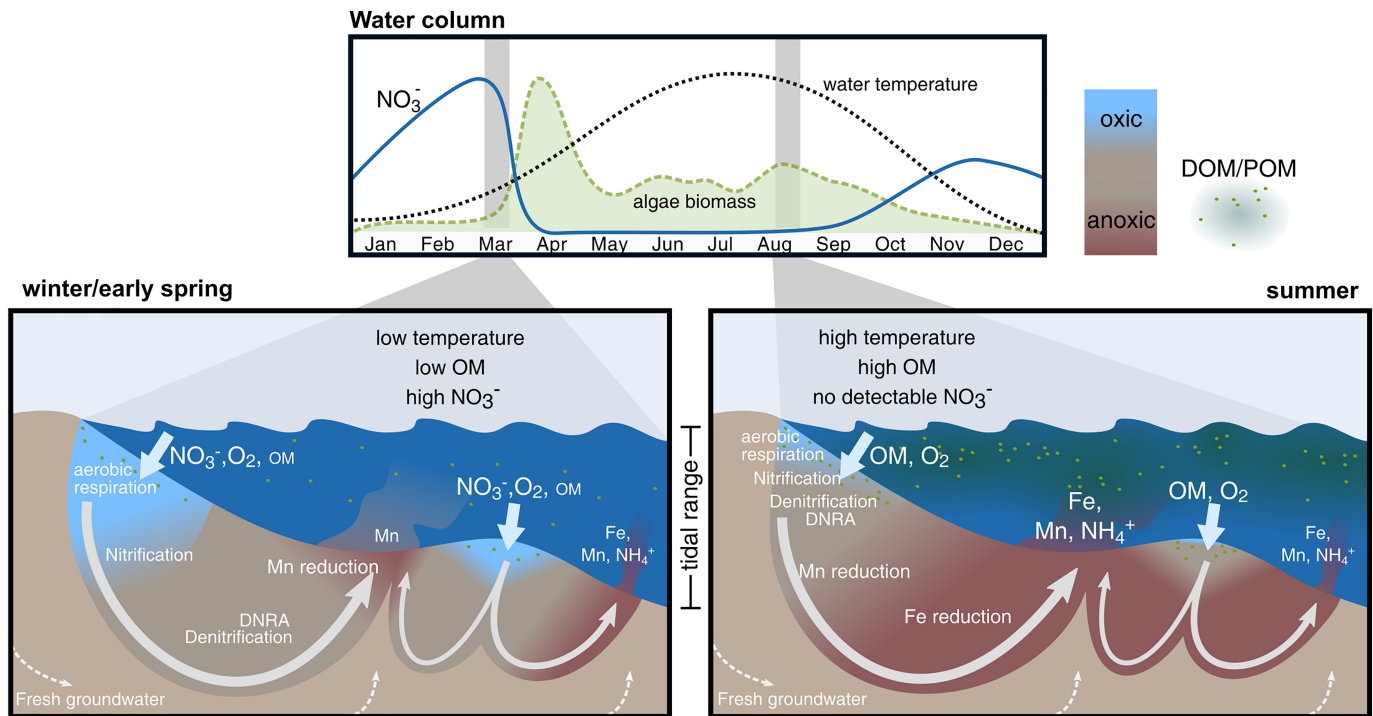
4.1.4. Seawater Temperature and Electron Acceptor Supply Governs OM Degradation

Due to continuous seawater infiltration, temperatures of saline pore waters were strongly coupled to pelagic water temperatures (Figure 4). O_2 consumption is strongly related to temperature and increases 1.8-fold for a 10°C rise in temperature (Thamdrup et al., 1998). Theoretically, a decrease in O_2 penetration by a factor of about 2 in August compared to March can be solely explained by the pore water temperature increase, assuming all other factors, for example, transport rates, to be constant. The current dataset does not allow to decide whether organic matter or temperature is the main driver for the shift in oxygen penetration depth. Besides for aerobic degradation rates, a temperature dependence has been observed for nitrate involving degradation pathways (Kaplan et al., 1977; Macfarlane & Herbert, 1984) and Mn and Fe reduction (Lovley et al., 2004; Nevin et al., 2005). However, these pathways are further controlled by oxygen presence or their respective electron acceptor availability (NO_3^- and Mn/Fe oxides).

Besides seasonal variability in electron donors and temperature, the supply of electron acceptors, like O_2 and NO_3^-, to beach sediments also varies seasonally (Figure 3). The infiltration of cold O_2- and nutrient-rich seawater from autumn to early spring promotes aerobic respiration and NO_3^- reduction (Froelich et al., 1979). In March, seawater O_2 concentration was about 20% higher compared to August (Figure 5a) due to higher gas solubility in colder seawater. Additionally, seawater NO_3^- concentration was higher in March compared to October and August (Figure 5b). The availability of NO_3^- is a controlling parameter stimulating nitrate reducing organic matter pathways, like denitrification (Deek et al., 2011). Hence, seawater in March supplied the highest quantity of the electron acceptors O_2 and NO_3^-, supporting aerobic respiration and nitrate reduction.

4.1.5. Effects of Changes in Beach Morphology

The redox zonation is also influenced by pore water flow paths and residence times, which are controlled by beach morphology and aquifer characteristics (McLachlan & Turner, 1994). A recent study at Spiekeroog beach emphasizes the coupling of beach morphology and subsurface pore water geochemistry (Waska et al., 2019). Thereafter, the intertidal morphology governs, where seawater constituents like O_2, organic matter, and seasonally NO_3^- infiltrate as well as where mineralization products discharge. Further, beach

Figure 10. Conceptual diagram of the coupling of biogeochemical dynamics in the water column and in intertidal sandy beach sediments. Seasonal variations in pelagic temperature, nutrient concentrations, and algae activity (upper panel; seawater temperature and algae biomass according to Meier et al., 2015) influence benthic microbial processes, and control pore water constituent effluxes. OM: dissolved organic matter (DOM) and particulate organic matter (POM). Oxic conditions (blue) include aerobic respiration and subsequent nitrification. Denitrification and dissimilatory nitrate reduction to ammonium (DNRA) are dominating in intermediate zones. Fe and Mn reduction is the most prominent process in anoxic zones (red). Thereby pore waters accumulate NH_4^+.

morphology affects the mixing of Fe-rich pore water with sulfidic fresh groundwater, which could lead to Fe precipitation (Waska et al., 2019). It is well known that beach morphology of north beach of Spiekeroog Island exhibits a seasonal dynamic (Waska et al., 2019), namely, a steep summer and a flat winter beach (Flemming & Davis, 1994). A seasonal imprint on pore water flow paths, thus, has to be considered as factor changing subsurface biogeochemistry.

4.2. Variability of Constituent Fluxes
4.2.1. Inorganic Nitrogen Fluxes

Flux calculations revealed that inorganic nitrogen species displayed the highest seasonal variability. The intertidal beach sediments behaved as net sink for NO_3^-, which was either transformed to gaseous species like N_2O or N_2, to dissolved NH_4^+ via DNRA and ammonification, or fixed in biomass. Predominantly from autumn to early spring, NO_3^- was transported into the intertidal subsurface with infiltrating seawater (Figures 3 and 8a). Concurrently, the efflux into surface waters was close to zero throughout the year (Figure 8a).

In contrast, NH_4^+ was generally exported from beach pore water to nearshore waters, due to intense microbial organic matter degradation. In October and March lower degradation rates compared to August caused lower net NH_4^+ fluxes. Additionally, higher seawater NH_4^+ input in March was decreasing the net efflux of NH_4^+ (Figure 8c). In August, higher microbial rates promoted anoxic conditions in the subsurface, which led to accumulating NH_4^+ in pore waters along the flow path. The August NH_4^+ net flux (121 mmol NH_4^+/day per meter shoreline) is comparable to reported May net fluxes at our study site (117 mmol NH_4^+/day per meter shoreline; Beck et al., 2017). Although the May fluxes might have been biased because samples of 50 cmbsf were used as end-members (Beck et al., 2017), it confirms that the onset of pelagic activity and rising temperatures in spring stimulated microbial activity in the intertidal subsurface. The trend to higher NH_4^+ fluxes in summer has also been observed in a recent study from Tolo Harbor, Hongkong,

yielding in comparable NH_4^+ fluxes of 115 mmol NH_4^+/day per meter shoreline in spring and 272 mmol NH_4^+/day per meter shoreline in summer (Liu et al., 2018). The authors concluded that the increase in summer net fluxes was stimulated by enhanced NH_4^+ production during organic matter degradation.

In a regional comparison with local tidal flats the release of NH_4^+ from intertidal beach sands in October (46 mmol NH_4^+/day per meter shoreline) is up to 20 times lower than the release from local backbarrier tidal flats in November (532–829 mmol NH_4^+/day per meter shoreline; Riedel et al., 2011). Combined with the lower spatial extension of beaches (Figure 1), it is obvious that beach sediments may contribute but are not the dominant NH_4^+ source to the coastal North Sea.

The high seasonal variability of the net DIN flux results from seasonal fluctuations in seawater NO_3^- inputs and variable effluxes of remineralized NH_4^+. Whereas the first is governed by pelagic algae biomass and other NO_3^- sinks, the latter mainly depends on microbial respiration rates. The temporal variability in DIN fluxes has been shown in prior studies (Couturier et al., 2017; Gonneea & Charette, 2014; Liu et al., 2018) where fluxes were in the same range as at our study site, ranging from 52 mmol DIN/day per meter shoreline (Gonneea & Charette, 2014) to 388 mmol DIN/day per meter shoreline (Couturier et al., 2017). However, a temporary net removal of DIN has not been observed in these environments. One main difference between Spiekeroog Island and Waquoit Bay (Cape Cod, USA; Gonneea & Charette, 2014), Martinique Beach (Gulf of St. Lawrence, Canada; Couturier et al., 2017), and Tolo Harbour (Hongkong; Liu et al., 2018) is the high tidal range of 2.7 m and the wave exposition of the Spiekeroog study site. Both potentially intensified the intertidal benthic-pelagic coupling and made the system sensitive to water column composition changes governing electron donor, electron acceptor supply and thus microbial rates. At Spiekeroog beach the net DIN flux for March yielded in an areal DIN loss rate of 16 $\mu mol/m^2$ per hour for the whole 160-m coast-perpendicular transect, solely based on DIN input and DIN output. When only the upper circulation cell (68 m) is taken into account, the rate increases to 48 $\mu mol/m^2$ per hour. These rates were in the same order as the calculated DIN loss of North Sea subtidal permeable sediments (22—94 $\mu mol/m^2$ per hour; Marchant et al., 2016) but were lower than N loss rates in intertidal sediments of the Wadden Sea (207 $\mu mol/m^2$ per hour; Gao et al., 2012). Due to the smaller spatial extension of sandy beaches compared to intertidal flat margins and subtidal sediments in the southern North Sea, the contribution of sandy beaches to N loss might be only minor in the southern North Sea. Additionally, net N loss is only suggested to be present in cold seasons, when seawater NO_3^- is high and microbial rates are comparably low. Nevertheless, beach sands contribute to N budgets in a regional context.

4.2.2. Mn and Fe Fluxes

The import of dissolved Mn must be considered for spring and autumn, when dissolved Mn concentrations in adjacent seawater have been reported to exceed 1 μM (Kowalski et al., 2012). However, the high concentrations of Mn have been identified to result from pore water derived Mn release in backbarrier tidal flats, after high organic matter input from algal blooms. It is thus more likely that intertidal beach sediments additionally govern coastal North Sea seawater Mn inventories. The flux of Mn was enhanced during summer when higher microbial rates and O_2 consumption led to more reducing conditions in pore waters (Figure 8b). In August, high Mn concentrations could even be observed in the upper circulation cell (Figure 6). As a consequence, Mn was exported into coastal surface waters. Oxidation within oxygenated surface sediment is unlikely due to high groundwater velocities of 0.3 to 0.7 m/day (Beck et al., 2017) and slow oxidation rates of Mn (Caetano et al., 1997).

Similar to Mn, the maximum Fe flux in August (Figure 8d) can be attributed to more reducing conditions in the beach sediments, especially in the upper circulation cell. The wide range of calculated fluxes is due to the high patchiness of dissolved Fe at 10 cmbsf (Figure 6). In pore waters dissolved Fe is mainly present as Fe^{2+}, but it oxidizes rapidly to particulate Fe when aerated seawater enters the sediment (Caetano et al., 1997). The lower Fe fluxes in comparison with 50-cmbsf-based Fe fluxes from Beck et al. (2017; Figure 8d) is most likely the result of an oxidation effect on 10 cmbsf Fe end-members of the current study. Nevertheless, due to the rapid oxidation of Fe, further oxidation in very surficial sediment depths must be considered and it is likely that potential Fe fluxes to coastal waters are still overestimated. Due to low sulfate reduction rates (Reckhardt et al., 2017), Fe is not sequestered in large quantities by dissolved sulfide at this site in contrast to other marine sites with intense sulfate reduction (McAllister et al., 2015; Roy et al., 2010). Therefore, the intertidal beach pore waters exhibit ideal conditions for Fe reduction and for the formation of Fe-rich pore

waters, which may be transported across the sediment-water interface, either by advective transport or by sediment erosion. Consequently, beach sediments of Spiekeroog Island must be considered as Fe and Mn source for the adjacent coastal ocean.

4.2.3. Constituent Mass Balances in Dynamic Intertidal Beaches

Constituent net fluxes have been shown to vary significantly on seasonal timescales (Figure 8) due to seasonal changes in subsurface biogeochemistry. The latter as well as pore water flow paths are influenced by steady sediment reallocation, storm surges, spring-neap tide cycles, and potential heterogeneities in sediment permeability. Furthermore, model-related uncertainties in volumetric fluxes have to be considered. Although subsurface flow heterogeneities were assumed to produce long-shore variabilities in salinity and temperature, the resulting biogeochemical patterns were predominantly governed by cross-shore systematics (Waska et al., 2019).

Model-related uncertainties in volumetric flux magnitudes have been integrated to flux calculations, which also accounted for different volumetric ratios of saline runnel and LWL exfiltration. Generally, such uncertainties will not change the ubiquitous mechanisms of the beach bioreactor based on a mass balance model of influx of seawater and the efflux of modified pore waters, which have been overprinted by organic matter degradation. At our study site, fluxes in the upper circulation cell are the main driver of total seasonal flux variations. It exhibits the highest volumetric exchange rates (Beck et al., 2017) and greatest variability in pore water biogeochemistry (Figures 6 and 7).

Uncertainties related to changes in flow paths have not been considered explicitly. Drastic changes, for example, the sole exfiltration of all infiltrating seawater at the LWL, principally could lead to wrong combinations of end-member and volumetric flux, but we can exclude such a flow path pattern based on intertidal head measurements (Beck et al., 2017; Waska et al., 2019). Additionally, pore water data of all transect replicates showed a comparable succession of electron acceptors, such as deep O_2 penetration at HWL, intermediate O_2 penetration at ridge sites, and very low oxygen penetration at runnel and LWL sites (Figures 6, 7, S5, S6, S7, and S8), which supports the underlain hydrogeological concept.

Flow path variabilities might increase the complexity of the organic matter degradation in intertidal sediments. Although potentially prone to errors, the presented constituent flux variability seems to be a robust estimation of how seasonal biogeochemical changes affect the fate of inorganic N, Fe, and Mn in intertidal high energy beach sediments.

5. Conclusions

The presented pore water data reveals that the interplay of benthic remineralization processes in intertidal pore waters and biological activity in adjacent coastal seawater affects organic matter degradation in intertidal permeable sediments. This, in turn, affects the composition of discharging fluids and thus constituent fluxes across the sediment-water interface. The main conclusions are visualized in Figure 10.

In the upper circulation cell, distinct vertical redox boundaries were found separating infiltration and exfiltration zones of seawater. Seasonal changes in temperature, organic matter, and electron acceptor availability (O_2, NO_3^-) affect microbial rates and respective electron acceptor utilization (Figure 10). The spatial distribution of organic matter degradation pathways, predominantly in the upper seawater circulation cell, affects pore water species and finally their flux across the sediment-water interface.

Net fluxes calculation of DIN species, Mn, and Fe showed seasonal variations by orders of magnitude. But fluxes may not only vary in magnitude. Beaches may even switch from sink to source, as shown for DIN. From autumn to early spring, seawater supplies high amounts of NO_3^-, low organic matter quantity, and quality, and thus microbial rates are considered to be low (Figure 10). During this time, aerobic and nitrate reducing organic matter degradation are most dominant and intertidal sediments can be an overall sink for seawater DIN. In contrast, seawater supplies very low amounts of NO_3^- and concurrently a high quantity and quality of fresh organic matter in summer. In combination with increased temperatures microbial rates are higher in summer. This creates spatially more extended anoxic conditions, promotes Mn and Fe reduction and enhances the release of NH_4^+ (Figure 10). As a consequence, pore waters provide recycled DIN, as NH_4^+, to coastal seawater in biologically active seasons and may thus refuel surface bioproductivity with

potentially limiting DIN species. In this respect beaches may be regarded as a buffer for DIN supply of the nearshore.

In the regional context, the imprint of DIN fluxes from barrier island beaches on nutrient budgets might be limited due to the large spatial extension of subtidal sediments and tidal flats, which release NH_4^+ as well. In contrast to DIN, barrier islands must be considered as Fe source to coastal seawater, although there are still uncertainties in the sediment-water interface Fe sequestration.

The results have implications for temporal constituent flux extrapolations of subterranean estuaries, which receive organic matter and DIN from overlying waters and which are affected by seasonal changes in pelagic activity. The overall impact of such subterranean estuaries on adjacent surface waters must be carefully assessed, considering flux variations or even the inversion of source or sink characteristics.

To date, high energy beach biogeochemistry has received only minor attention, regarding nutrient and metal fluxes although these beach types are widespread along global coastlines. For example, the effect of steady beach sediment redistribution is not yet constrained with respect to dissolved constituent and suspended matter export and should be subject to future studies.

References

Ahmerkamp, S., Winter, C., Krämer, K., de Beer, D., Janssen, F., Friedrich, J., et al. (2017). Regulation of benthic oxygen fluxes in permeable sediments of the coastal ocean. *Limnology and Oceanography*, *62*(5), 1935–1954. https://doi.org/10.1002/lno.10544

Ahrens, J., Beck, M., Marchant, H. K., Ahmerkamp, S., Schnetger, B., & Brumsack, H.-J. (2019). *Seasonal oxygen, nutrient, Mn, and Fe data for intertidal pore waters and adjacent seawater of Spiekeroog Island North Beach* (Germany). PANGAEA - Data Publisher for Earth & Environmental Science. https://doi.org/10.1594/PANGAEA.905932

Anschutz, P., Smith, T., Mouret, A., Deborde, J., Bujan, S., Poirier, D., & Lecroart, P. (2009). Tidal sands as biogeochemical reactors. *Estuarine, Coastal and Shelf Science*, *84*(1), 84–90. https://doi.org/10.1016/j.ecss.2009.06.015

Antia, E. (1995). Sedimentary deposits related to inlet-shoreface storm flow interaction in the German Bight. *Estuarine, Coastal and Shelf Science*, *40*(6), 699–712. https://doi.org/10.1006/ecss.1995.0047

Beck, A. J., Tsukamoto, Y., Tovar-Sanchez, A., Huerta-Diaz, M., Bokuniewicz, H. J., & Sañudo-Wilhelmy, S. A. (2007). Importance of geochemical transformations in determining submarine groundwater discharge-derived trace metal and nutrient fluxes. *Applied Geochemistry*, *22*(2), 477–490. https://doi.org/10.1016/j.apgeochem.2006.10.005

Beck, M., & Brumsack, H.-J. (2012). Biogeochemical cycles in sediment and water column of the Wadden Sea: The example Spiekeroog Island in a regional context. *Ocean and Coastal Management*, *68*, 102–113. https://doi.org/10.1016/j.ocecoaman.2012.05.026

Beck, M., Köster, J., Engelen, B., Holstein, J. M., Gittel, A., Könneke, M., et al. (2009). Deep pore water profiles reflect enhanced microbial activity towards tidal flat margins. *Ocean Dynamics*, *59*(2), 371–383. https://doi.org/10.1007/s10236-008-0176-z

Beck, M., Reckhardt, A., Amelsberg, J., Bartholomä, A., Brumsack, H.-J., Cypionka, H., et al. (2017). The drivers of biogeochemistry in beach ecosystems: A cross-shore transect from the dunes to the low-water line. *Marine Chemistry*, *190*, 35–50. https://doi.org/10.1016/j.marchem.2017.01.001

Benesch, R., & Mangelsdorf, P. (1972). Eine Methode zur colorimetrischen Bestimmung von Ammoniak in Meerwasser. *Helgoländer Wissenschaftliche Meeresuntersuchungen*, *23*(3), 365–375. https://doi.org/10.1007/bf01609682

Billerbeck, M., Werner, U., Bosselmann, K., Walpersdorf, E., & Huettel, M. (2006). Nutrient release from an exposed intertidal sand flat. *Marine Ecology Progress Series*, *316*, 35–51. https://doi.org/10.3354/meps316035

Caetano, M., Falcão, M., Vale, C., & Bebianno, M. (1997). Tidal flushing of ammonium, iron and manganese from inter-tidal sediment pore waters. *Marine Chemistry*, *58*(1-2), 203–211. https://doi.org/10.1016/s0304-4203(97)00035-2

Charbonnier, C., Anschutz, P., Deflandre, B., Bujan, S., & Lecroart, P. (2016). Measuring pore water oxygen of a high-energy beach using buried probes. *Estuarine, Coastal and Shelf Science*, *179*, 66–78. https://doi.org/10.1016/j.ecss.2015.12.004

Charbonnier, C., Anschutz, P., Poirier, D., Bujan, S., & Lecroart, P. (2013). Aerobic respiration in a high-energy sandy beach. *Marine Chemistry*, *155*, 10–21. https://doi.org/10.1016/j.marchem.2013.05.003

Cline, J. D. (1969). Spectrophotometric determination of hydrogen sulfide in natural waters. *Limnology and Oceanography*, *14*(3), 454–458. https://doi.org/10.4319/lo.1969.14.3.0454

Couturier, M., Tommi-Morin, G., Sirois, M., Rao, A., Nozais, C., & Chaillou, G. (2017). Nitrogen transformations along a shallow subterranean estuary. *Biogeosciences*, *14*(13), 3321–3336. https://doi.org/10.5194/bg-14-3321-2017

Deek, A., Emeis, K., & van Beusekom, J. (2011). Nitrogen removal in coastal sediments of the German Wadden Sea. *Biogeochemistry*, *108*(1-3), 467–483. https://doi.org/10.1007/s10533-011-9611-1

Dette, H.-H. (1977). Ein Vorschlag zur Analyse eines Wellenklimas. *Die Küste*, *31*, 166–180. https://hdl.handle.net/20.500.11970/101117

Flemming, B. W. (2005). *Tidal Environments* (pp. 954–958). Dordrecht, Netherlands: Springer. https://doi.org/10.1007/1-4020-3880-1_315

Flemming, B. W., & Davis, R. A. Jr. (1994). Holocene evolution, morphodynamics and sedimentology of the Spiekeroog barrier island system (southern North Sea). *Senckenbergiana Maritima*, *24*, 117–155.

Froelich, P., Klinkhammer, G., Bender, M., Luedtke, N., Heath, G., Cullen, D., et al. (1979). Early oxidation of organic matter in pelagic sediments of the eastern equatorial Atlantic: Suboxic diagenesis. *Geochimica et Cosmochimica Acta*, *43*(7), 1075–1090. https://doi.org/10.1016/0016-7037(79)90095-4

Gao, H., Matyka, M., Liu, B., Khalili, A., Kostka, J. E., Collins, G., et al. (2012). Intensive and extensive nitrogen loss from intertidal permeable sediments of the Wadden Sea. *Limnology and Oceanography*, *57*(1), 185–198. https://doi.org/10.4319/lo.2012.57.1.0185

Garcia, H. E., & Gordon, L. I. (1992). Oxygen solubility in seawater: Better fitting equations. *Limnology and Oceanography*, *37*(6), 1307–1312. https://doi.org/10.4319/lo.1992.37.6.1307

Gonneea, M. E., & Charette, M. A. (2014). Hydrologic controls on nutrient cycling in an unconfined coastal aquifer. *Environmental Science & Technology*, *48*(24), 14,178–14,185. https://doi.org/10.1021/es503313t

Grasshoff, K., Kremling, K., & Ehrhardt, M. (Eds.) (1999). *Methods of Seawater Analysis*. Weinheim, Germany: Wiley-VCH.

Grunwald, M., Dellwig, O., Kohlmeier, C., Kowalski, N., Beck, M., Badewien, T. H., et al. (2010). Nutrient dynamics in a back barrier tidal basin of the Southern North Sea: Time-series, model simulations, and budget estimates. *Journal of Sea Research*, *64*(3), 199–212. https://doi.org/10.1016/j.seares.2010.02.008

Hedges, J. I., Clark, W. A., & Come, G. L. (1988). Fluxes and reactivities of organic matter in a coastal marine bay. *Limnology and Oceanography*, *33*(5), 1137–1152. https://doi.org/10.4319/lo.1988.33.5.1137

Heiss, J. W., Post, V. E. A., Laattoe, T., Russoniello, C. J., & Michael, H. A. (2017). Physical controls on biogeochemical processes in intertidal zones of beach aquifers. *Water Resources Research*, *53*(11), 9225–9244. https://doi.org/10.1002/2017WR021110

Hubaux, A., & Vos, G. (1970). Decision and detection limits for calibration curves. *Analytical Chemistry*, *42*(8), 849–855. https://doi.org/10.1021/ac60290a013

Huettel, M., Berg, P., & Kostka, J. E. (2014). Benthic exchange and biogeochemical cycling in permeable sediments. *Annual Review of Marine Science*, *6*(1), 23–51. https://doi.org/10.1146/annurev-marine-051413-012706

Huettel, M., & Rusch, A. (2000a). Advective particle transport into permeable sediments-evidence from experiments in an intertidal sandflat. *Limnology and Oceanography*, *45*(3), 525–533. https://doi.org/10.4319/lo.2000.45.3.0525

Huettel, M., & Rusch, A. (2000b). Transport and degradation of phytoplankton in permeable sediment. *Limnology and Oceanography*, *45*(3), 534–549. https://doi.org/10.4319/lo.2000.45.3.0534

Huettel, M., Ziebis, W., Forster, S., & Luther, G. W. (1998). Advective transport affecting metal and nutrient distributions and interfacial fluxes in permeable sediments. *Geochimica et Cosmochimica Acta*, *62*(4), 613–631. https://doi.org/10.1016/s0016-7037(97)00371-2

Johannsen, A., Dähnke, K., & Emeis, K. (2008). Isotopic composition of nitrate in five German rivers discharging into the North Sea. *Organic Geochemistry*, *39*(12), 1678–1689. https://doi.org/10.1016/j.orggeochem.2008.03.004

Jørgensen, B., & Sørensen, J. (1985). Seasonal cycles of O_2, NO_3^- and SO_4^{2-} reduction in estuarine sediments: The significance of an NO_3^- reduction maximum in spring. *Marine Ecology Progress Series*, *24*, 65–74. https://doi.org/10.3354/meps024065

Kaplan, W. A., Teal, J. M., & Valiela, I. (1977). Denitrification in salt marsh sediments: Evidence for seasonal temperature selection among populations of denitrifiers. *Microbial Ecology*, *3*(3), 193–204. https://doi.org/10.1007/bf02010617

Kim, K. H., Heiss, J. W., Michael, H. A., Cai, W.-J., Laattoe, T., Post, V. E. A., & Ullman, W. J. (2017). Spatial patterns of groundwater biogeochemical reactivity in an intertidal beach aquifer. *Journal of Geophysical Research: Biogeosciences*, *122*, 2548–2562. https://doi.org/10.1002/2017JG003943

Kim, K. H., Michael, H. A., Field, E. K., & Ullman, W. J. (2019). Hydrologic shifts create complex transient distributions of particulate organic carbon and biogeochemical responses in beach aquifers. *Journal of Geophysical Research: Biogeosciences*, *124*, 3024–3038. https://doi.org/10.1029/2019JG005114

Kowalski, N., Dellwig, O., Beck, M., Grunwald, M., Dürselen, C.-D., Badewien, T. H., et al. (2012). A comparative study of manganese dynamics in the water column and sediments of intertidal systems of the North Sea. *Estuarine, Coastal and Shelf Science*, *100*, 3–17. https://doi.org/10.1016/j.ecss.2011.03.011

Liu, Y., Jiao, J. J., Liang, W., & Luo, X. (2017). Tidal Pumping-Induced Nutrients Dynamics and Biogeochemical Implications in an Intertidal Aquifer. *Journal of Geophysical Research: Biogeosciences*, *122*, 3322–3342. https://doi.org/10.1002/2017JG004017

Liu, Y., Liang, W., & Jiao, J. J. (2018). Seasonality of nutrient flux and biogeochemistry in an intertidal aquifer. *Journal of Geophysical Research: Oceans*, *123*, 6116–6135. https://doi.org/10.1029/2018JC014197

Lovley, D. R., Holmes, D. E., & Nevin, K. P. (2004). Dissimilatory Fe(III) and Mn(IV) reduction. *Advances in Microbial Physiology*, *49*, 219–286. https://doi.org/10.1016/S0065-2911(04)49005-5

Luijendijk, A., Hagenaars, G., Ranasinghe, R., Baart, F., Donchyts, G., & Aarninkhof, S. (2018). The state of the world's beaches. *Scientific Reports*, *8*(1), 6641. https://doi.org/10.1038/s41598-018-24630-6

Luther, G. W., Sundby, B., Lewis, B. L., Brendel, P. J., & Silverberg, N. (1997). Interactions of manganese with the nitrogen cycle: Alternative pathways to dinitrogen. *Geochimica et Cosmochimica Acta*, *61*(19), 4043–4052. https://doi.org/10.1016/s0016-7037(97)00239-1

Macfarlane, G., & Herbert, R. (1984). Effect of oxygen tension, salinity, temperature and organic matter concentration on the growth and nitrifying activity of an estuarine strain of Nitrosomonas. *FEMS Microbiology Letters*, *23*(1), 107–111. https://doi.org/10.1111/j.1574-6968.1984.tb01044.x

Marchant, H. K., Ahmerkamp, S., Lavik, G., Tegetmeyer, H. E., Graf, J., Klatt, J. M., et al. (2017). Denitrifying community in coastal sediments performs aerobic and anaerobic respiration simultaneously. *The ISME Journal*, *11*(8), 1799–1812. https://doi.org/10.1038/ismej.2017.51

Marchant, H. K., Holtappels, M., Lavik, G., Ahmerkamp, S., Winter, C., & Kuypers, M. M. M. (2016). Coupled nitrification-denitrification leads to extensive N loss in subtidal permeable sediments. *Limnology and Oceanography*, *61*(3), 1033–1048. https://doi.org/10.1002/lno.10271

Marchant, H. K., Lavik, G., Holtappels, M., & Kuypers, M. M. M. (2014). The fate of nitrate in intertidal permeable sediments. *PLoS ONE*, *9*(8), e104517. https://doi.org/10.1371/journal.pone.0104517

Marchant, H. K., Tegetmeyer, H. E., Ahmerkamp, S., Holtappels, M., Lavik, G., Graf, J., et al. (2018). Metabolic specialization of denitrifiers in permeable sediments controls N_2O emissions. *Environmental Microbiology*, *20*(12), 4486–4502. https://doi.org/10.1111/1462-2920.14385

McAllister, S. M., Barnett, J. M., Heiss, J. W., Findlay, A. J., MacDonald, D. J., Dow, C. L., et al. (2015). Dynamic hydrologic and biogeo-chemical processes drive microbially enhanced iron and sulfur cycling within the intertidal mixing zone of a beach aquifer. *Limnology and Oceanography*, *60*(1), 329–345. https://doi.org/10.1002/lno.10029

McLachlan, A. (1982). A model for the estimation of water filtration and nutrient regeneration by exposed sandy beaches. *Marine Environmental Research*, *6*(1), 37–47. https://doi.org/10.1016/0141-1136(82)90006-x

McLachlan, A., & Turner, I. (1994). The interstitial environment of sandy beaches. *Marine Ecology*, *15*(3-4), 177–212. https://doi.org/10.1111/j.1439-0485.1994.tb00053.x

Meier, S., Muijsers, F., Beck, M., Badewien, T. H., & Hillebrand, H. (2015). Dominance of the non-indigenous diatom Mediopyxis helysia in Wadden Sea phytoplankton can be linked to broad tolerance to different Si and N supplies. *Journal of Sea Research*, *95*, 36–44. https://doi.org/10.1016/j.seares.2014.10.001

Michael, H. A., Mulligan, A. E., & Harvey, C. F. (2005). Seasonal oscillations in water exchange between aquifers and the coastal ocean. *Nature*, *436*(7054), 1145–1148. https://doi.org/10.1038/nature03935

Nevin, K. P., Holmes, D. E., Woodard, T. L., Hinlein, E. S., Ostendorf, D. W., & Lovley, D. R. (2005). Geobacter bemidjiensis sp. nov. and Geobacter psychrophilus sp. nov., two novel Fe(III)-reducing subsurface isolates. *International Journal of Systematic and Evolutionary Microbiology*, *55*(4), 1667–1674. https://doi.org/10.1099/ijs.0.63417-0

O'Connor, A. E., Krask, J. L., Canuel, E. A., & Beck, A. J. (2018). Seasonality of major redox constituents in a shallow subterranean estuary. *Geochimica et Cosmochimica Acta*, *224*, 344–361. https://doi.org/10.1016/j.gca.2017.10.013

O'Connor, A. E., Luek, J. L., McIntosh, H., & Beck, A. J. (2015). Geochemistry of redox-sensitive trace elements in a shallow subterranean estuary. *Marine Chemistry*, *172*, 70–81. https://doi.org/10.1016/j.marchem.2015.03.001

Reckhardt, A., Beck, M., Greskowiak, J., Schnetger, B., Böttcher, M. E., Gehre, M., & Brumsack, H.-J. (2017). Cycling of redox-sensitive elements in a sandy subterranean estuary of the southern North Sea. *Marine Chemistry*, *188*, 6–17. https://doi.org/10.1016/j.marchem.2016.11.003

Reckhardt, A., Beck, M., Seidel, M., Riedel, T., Wehrmann, A., Bartholomä, A., et al. (2015). Carbon, nutrient and trace metal cycling in sandy sediments: A comparison of high-energy beaches and backbarrier tidal flats. *Estuarine, Coastal and Shelf Science*, *159*, 1–14. https://doi.org/10.1016/j.ecss.2015.03.025

Riedel, T., Lettmann, K., Schnetger, B., Beck, M., & Brumsack, H.-J. (2011). Rates of trace metal and nutrient diagenesis in an intertidal creek bank. *Geochimica et Cosmochimica Acta*, *75*(1), 134–147. https://doi.org/10.1016/j.gca.2010.09.040

Robinson, C. E., Xin, P., Santos, I. R., Charette, M. A., Li, L., & Barry, D. (2018). Groundwater dynamics in subterranean estuaries of coastal unconfined aquifers: Controls on submarine groundwater discharge and chemical inputs to the ocean. *Advances in Water Resources*, *115*, 315–331. https://doi.org/10.1016/j.advwatres.2017.10.041

Röper, T., Kröger, K. F., Meyer, H., Sültenfuss, J., Greskowiak, J., & Massmann, G. (2012). Groundwater ages, recharge conditions and hydrochemical evolution of a barrier island freshwater lens (Spiekeroog, Northern Germany). *Journal of Hydrology*, *454-455*, 173–186. https://doi.org/10.1016/j.jhydrol.2012.06.011

Roy, M., Martin, J. B., Cherrier, J., Cable, J. E., & Smith, C. G. (2010). Influence of sea level rise on iron diagenesis in an east Florida subterranean estuary. *Geochimica et Cosmochimica Acta*, *74*(19), 5560–5573. https://doi.org/10.1016/j.gca.2010.07.007

Santos, I. R., Burnett, W. C., Dittmar, T., Suryaputra, I. G., & Chanton, J. (2009). Tidal pumping drives nutrient and dissolved organic matter dynamics in a Gulf of Mexico subterranean estuary. *Geochimica et Cosmochimica Acta*, *73*(5), 1325–1339. https://doi.org/10.1016/j.gca.2008.11.029

Santos, I. R., Eyre, B. D., & Huettel, M. (2012). The driving forces of porewater and groundwater flow in permeable coastal sediments: A review. *Estuarine, Coastal and Shelf Science*, *98*, 1–15. https://doi.org/10.1016/j.ecss.2011.10.024

Schnetger, B., & Lehners, C. (2014). Determination of nitrate plus nitrite in small volume marine water samples using vanadium(III) chloride as a reduction agent. *Marine Chemistry*, *160*, 91–98. https://doi.org/10.1016/j.marchem.2014.01.010

Seibert, S. L., Holt, T., Reckhardt, A., Ahrens, J., Beck, M., Pollmann, T., et al. (2018). Hydrochemical evolution of a freshwater lens below a barrier island (Spiekeroog, Germany): The role of carbonate mineral reactions, cation exchange and redox processes. *Applied Geochemistry*, *92*, 196–208. https://doi.org/10.1016/j.apgeochem.2018.03.001

Seidel, M., Beck, M., Greskowiak, J., Riedel, T., Waska, H., Suryaputra, I., et al. (2015). Benthic-pelagic coupling of nutrients and dissolved organic matter composition in an intertidal sandy beach. *Marine Chemistry*, *176*, 150–163. https://doi.org/10.1016/j.marchem.2015.08.011

Shaw, T. J., Gieskes, J. M., & Jahnke, R. A. (1990). Early diagenesis in differing depositional environments: The response of transition metals in pore water. *Geochimica et Cosmochimica Acta*, *54*(5), 1233–1246. https://doi.org/10.1016/0016-7037(90)90149-f

Shum, K., & Sundby, B. (1996). Organic matter processing in continental shelf sediments—the subtidal pump revisited. *Marine Chemistry*, *53*(1-2), 81–87. https://doi.org/10.1016/0304-4203(96)00014-x

Thamdrup, B., Hansen, J. W., & Jørgensen, B. B. (1998). Temperature dependence of aerobic respiration in a coastal sediment. *FEMS Microbiology Ecology*, *25*(2), 189–200. https://doi.org/10.1111/j.1574-6941.1998.tb00472.x

Van Raaphorst, W., Kloosterhuis, H. T., Cramer, A., & Bakker, K. J. (1990). Nutrient early diagenesis in the sandy sediments of the dogger bank area, North Sea: Pore water results. *Netherlands Journal of Sea Research*, *26*(1), 25–52. https://doi.org/10.1016/0077-7579(90)90054-k

Waska, H., Greskowiak, J., Ahrens, J., Beck, M., Ahmerkamp, S., Böning, P., et al. (2019). Spatial and temporal patterns of pore water chemistry in the inter-tidal zone of a high energy beach. *Frontiers in Marine Science*, *6*(154), 1–12. https://doi.org/10.3389/fmars.2019.00154

Wessel, P., Smith, W. H. F., Scharroo, R., Luis, J., & Wobbe, F. (2013). Generic Mapping Tools: Improved version released. *Eos, Transactions American Geophysical Union*, *94*(45), 409–410. https://doi.org/10.1002/2013eo450001

Xin, P., Robinson, C., Li, L., Barry, D. A., & Bakhtyar, R. (2010). Effects of wave forcing on a subterranean estuary. *Water Resources Research*, *46*, W12505. https://doi.org/10.1029/2010WR009632